D3: Lunar Photometer Calibration for Lunar Spectral Irradiance Measurements

ABSTRACT

This document presents the calibration process for the CIMEL 318-TP9 for use in obtaining lunar irradiance measurements and discusses the results of the calibration and characterisation performed. This document presents the calibration process for the CIMEL and discusses the results of the calibration and characterisation performed. This document presents the calibration process for the CIMEL 318-TP9 for use in obtaining lunar irradiance measurements and discusses the results of the calibration and characterisation performed. 318-TP9 for use in obtaining lunar irradiance measurements

Sarah Taylor, Claire Greenwell, Emma Woolliams

National Physical Laboratory

12th December 2018

This document was produced as part of the ESA-funded project “Lunar spectral irradiance measurement and modelling for absolute calibration of EO optical sensors” under ESA contract number: 4000121576/17/NL/AF/hh

esa NPL National Physical Laboratory vito Universidad de Valladolid

Signatures and version history

	Name	Organisation	Date
Written by	Claire Greenwell	NPL	June 2018
Written by	Sarah Taylor	NPL	December 2018
Written by	Emma Woolliams	NPL	December 2018
Reviewed by (consortium)	N/A		
Approved by (ESA)	Marc Bouvet	ESA	January 2019

Version history

Version	Date	Publicly available or private to consortium?
1	January 2019	Private

Contents

1 Introduction

1.1 Purpose and Scope

This document forms deliverable D3 of the ESA project: "Lunar spectral irradiance measurement and modelling for absolute calibration of EO optical sensors".

This document presents the calibration process for the CIMEL 318-TP9 and discusses the results of the calibration and characterisation performed.

1.2 Applicable and reference documents

Number	Reference
D1	Strategy for the Derivation of an Improved Spectral Irradiance Model Based on Lunar Photometer Measurements
D2	Lunar Spectral Irradiance Measurement Protocol from a Lunar Photometer
D4	Lunar Spectral Irradiance Measurement Uncertainties from a Lunar Photometer
D5	Operation and Maintenance Manual for Lunar Photometer
D6	Lunar Spectral Irradiance Retrieval from the Lunar Photometer Measurements

Scientific references are provided in Section 9.

1.3 Glossary

1.3.1 Abbreviations

Abbreviation	Stands For	Notes
Cimel	(Not an abbreviation)	Instrument manufacturer, also used as shorthand for instrument itself
EO	Earth Observation	
ESA	European Space Agency	Project customer
FEL	(Not an abbreviation)	An ANSI designation for a particular form of double coiled 1000 W tungsten halogen lamp often used as an irradiance standard
FOV	Field of View	
GIRO	GSICS Implementation of the ROLO Model	
GSICS	Global Space Based Inter-calibration System	
GUM	Guide for the Expression of Uncertainty	
InGaAs	Inidium Gallium Arsenide	
ML	Miner's Lamp	
NLU	CIMEL scenario for direct Moon Triplet	
NPL	National Physical Laboratory	Project partner
PLU	CIMEL scenario for polarized direct moon	
ROLO	RObotic Lunar Observatory	
Si	Silicon	
TOA	Top of Atmosphere	
UVa	University of Valladolid	Project partner
VITO	Vlaamse Instelling voor Technologisch Onderzoek; Flemish Institute for Technological Research	Project partner

2 Scientific Background

2.1 Project Aim

The Moon makes an ideal reference site for EO radiometric calibration as it is free from the atmospheric interference inherent in terrestrial calibration sites, and is largely photometrically stable However, use of the Moon has its own unique challenges largely due to the absolute irradiance of the Moon varying with the phase angle over a month, and libration over 18 years.

The main objective of this project is to use ground based measurements taken with a lunar photometer to improve upon previous modelling of the lunar disk irradiance variations through its cycles (to <2 % uncertainty). Because the measurements will only be taken over a small fraction of the lunar libration cycle, we will supplement the model with existing information including previous observations and the information within previous lunar irradiance ROLO/GIRO model.

Barreto et al (Barreto, 2016) have provided initial evidence that lunar photometers can be used as a reliable method to acquire the measurements required to calculate extra-terrestrial lunar irradiance, and that this method could lead to improvement in the accuracy and temporal frequency of lunar irradiance measurements.

By taking repeated measurements from a location with low atmospheric aerosol content, and correcting these measurements for atmospheric interference by the Langley method, the straight line fit can be extrapolated to $m = 0$ (where m= air mass), to obtain TOA signal. This signal when multiplied by the appropriate calibration coefficient provides lunar irradiance that would be observed by an instrument placed above the atmosphere (see project Deliverable D6 for further information on the retrieval of lunar irradiance from Lunar photometer measurements).

Essential to the retrieval of lunar irradiance measurement using such a lunar photometer is the detailed characterisation of the properties of the instrument. It is essential in particular to confirm the instrument is linear, due to the wide dynamic range of signal the instrument needs to measure through the lunar cycle (see section 5); an assessment of the thermal sensitivity of the instrument is required due to the wide variation in measurement site ambient temperature and temperature correction quantified (see section 4); and the spectral irradiance calibration coefficients at the spectral range of each filter must be calculated to allow conversion from signal voltage to absolute irradiance (see section 7).

2.2 Instrument

The Instrument used in this project is the CIMEL 318-TP9. This instrument meets many of the requirements as set out in project deliverable D1. The CIMEL is designed for 95 % stray light rejection with scattering angle of 2.5° ((Holben et al., 2002) , it has the necessary tracking capability and the dynamic range and linearity needed to cover both solar and lunar observations. It also has built in polarisation measurement capability. It come with 9 standard filters 340, 380, 440, 500, 675, 870, 937, 1020, 1640 nm, and is equipped with 2 detectors in the sensor head: Silicon and InGaAs. The 1020 filter is use in both the Si and InGaAs detectors (1020i refers to the InGaAs measurements in this document).

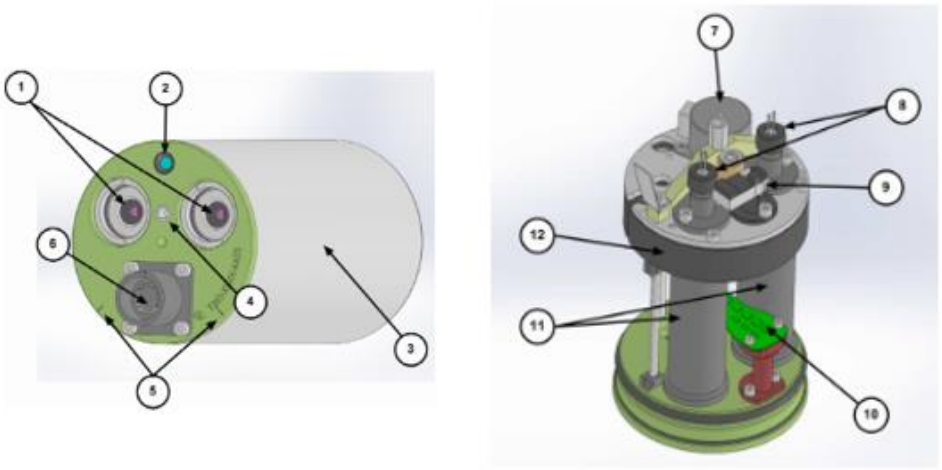

Figure 1: Internal diagram of photometer

1. Front plate lenses and optical chambers entrance
2. 4 quadrant detector lens
3. Cover
4. Threaded hole for collimator
5. Positioning notches
6. Head sensor cord connector
7. Step by step motor
8. Detectors
9. Filter wheel detector
10. 4 quadrant
11. Optical chambers
12. Filter wheel carter

2.2.1 Collimator

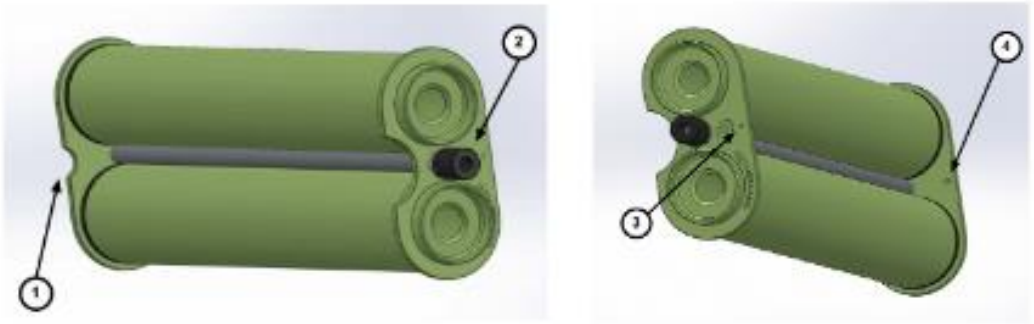

1: notch

2: tightening screw

3: alignment hole

Figure 2: photometer "collimators"

From the manual: the collimator is a component that enables the light to be guided correctly to the sensor head outside lenses. The collimator helps to reduce the stray light. The calibration was performed with the collimators attached as this is how the instrument is used in the field.

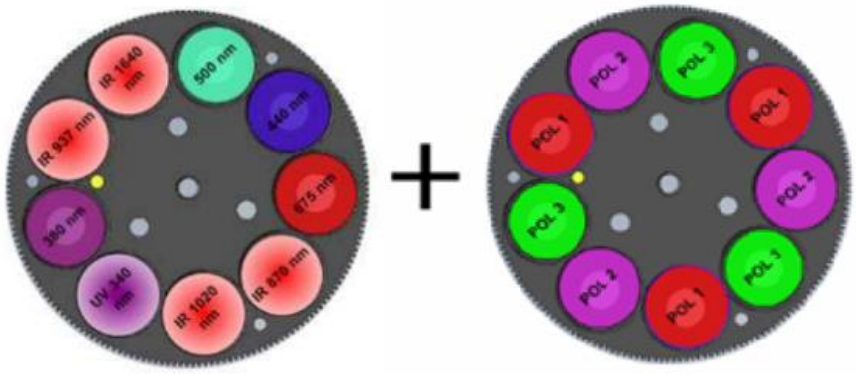

Figure 3: Filter wheel and polariser wheel (ref. manual)

2.2.2 Gains and scenarios

The instrument operates using a number of different "scenarios". These are automatic programs that define the movements of the robots and the sources that are observed, as well as setting appropriate gains for different observations. The electrical gains are set depending on the source irradiance, so the SUN gain is the lowest, and MOON and SKY gain the highest, with AUREOLE in between.

Although the instrument is used to measure irradiance and radiance, apart from the electronic gains there is no any other difference in the instrument operation between the different scenarios. For the irradiance type measurements Sun and Moon it is crucial to ensure that the FOV is not overfilled by the size of the source. This feature of the sun photometer is useful in situ to transfer the calibration coefficients between irradiance and radiance using the accurate knowledge of the solid angle penetrating the field of view of the instrument.

It is important to note that the SKY and AUREOLE scenarios are defined to carry out radiance measurements and that the irradiance calibration coefficients are thus inappropriate. It is possible to use the relationship between the irradiance and radiance measurement with the instrument solid angle to determine the necessary radiance calibration coefficients by using equation 1.

$$\boldsymbol{\Omega_v = \frac{E(\lambda)}{L(\lambda)} = \frac{C_{Ea}(\lambda)V_{Ea}(\lambda)}{C_{La}(\lambda)V_{La}(\lambda)}} \qquad \textit{Equation 1}$$

Where: Ω_v is the solid angle of the instrument field of view, $E(\lambda)$ is the irradiance at a given wavelength λ, $L(\lambda)$ is radiance, $C_{Ea}(\lambda)$ is what would be the irradiance calibration coefficient for AUREOLE mode , $V_{Ea}(\lambda)$ is the instrument signal recorded during irradiance calibration, $C_{La}(\lambda)$ is a AUREOLE mode absolute radiometric calibration coefficient and $V_{La}(\lambda)$ is an instrument signal recorded at this mode.

Knowledge of the following ratios between electrical gains will be useful for validation of the characterisation results

SUN/MOON or SUN/SKY	= 4096
SUN/AUR	= 128
AUR/MOON or AUR/SKY	= 32
MOON/SKY	= 1

2.2.3 Measurement Scenarios and filter lists

MOON

"day","time","K_1020","K_1640","K_870","K_675","K_440","K_500","K_1020i","K_935","K_380","K_340","temp"

SUN

"day","time","S_1020","S_1640","S_870","S_675","S_440","S_500","S_1020i","S_935","S_380","S_340","temp"

SKY

"day","time","A_1020","A_1640","A_870","A_675","A_440","A_500","A_380","A_340","K_1020","KP1_1020","KP2_1020","KP3_1020","K_1640","KP1_1640","KP2_1640","KP3_1640","K_870","KP1_870","KP2_870","KP3_870","K_675","KP1_675","KP2_675","KP3_675","K_440","KP1_440","KP2_440","KP3_440","K_500","KP1_500","KP2_500","KP3_500","K_380","KP1_380","KP2_380","KP3_380","K_340","KP1_340","KP2_340","KP3_340","temp"

A more in depth description of the CIMEL scenarios used in the project is found in deliverable D2

3 Characterisation of the Instrument

3.1 Summary of characterisation and calibration tests performed

3.1.1 Temperature Sensitivity:

The temperature sensitivity characterisation was carried out by UVa. Two sets of measurements have been performed in the UVa thermal chamber, where the CIMEL sensor head performs measurements on NLU[1]/ PLU[2] scenarios at temperatures ranging from 50 °C to -40 °C during a period of 4 hours, which is a rate of change of about 0.3 °C/min:

- In December 2017 one set of measurements in NLU only.
- In January 2018 both NLU and PLU.

The coefficients represent a correction of the signal to make it as though the measurements were taken at 25degC.

3.1.2 Linearity

The linearity of the CIMEL was assessed on the MOON gain only in the NPL linearity facility. A linearity factor for each filter has been assessed. The average linearity factor for each is listed in section 5.2

3.1.3 Irradiance Responsivity

Irradiance calibration coefficients for all filters on the MOON gain were determined by two methods. Firstly a calibration against a miner's lamp – an uncalibrated source, with calibrations transferred from a calibrated FEL lamp, via a transfer spectrometer. Results are presented in section 7.4.

Secondly, calibration coefficients obtained by direct calibration against the FEL lamp on SUN, AUR and SKY gains (section 7.2) have been used to verify the electrical ratio between gains (See Appendix 9A.1). These electrical gains have been used to validate the coefficients from the miner's lamp calibration and determine coefficients for those filters not covered by the miner's lamp (section 7.5)

Temperature correction has been applied to all raw data using the September 2018 coefficients provided by UVa.

3.1.4 Radiance Responsivity

The CIMEL radiometer can make measurements of both irradiance and radiance. Only the irradiance measurements are used in this project. However, because UVa uses radiance measurements as part of its quality assurance and instrument calibration, NPL also determined radiance calibration coefficients for comparison with the UVa calibration.

Radiance calibration coefficients for MOON / SKY gain were calculated using a lamp-diffuser tile combination on the NPL 8 m bench. 2 FEL lamps were used with 2 repeats performed on each of the Si and InGaAs detectors. Temperature correction was applied to all the data using the September 2018 coefficients provided by UVa.

A comparison with calibration coefficients calculated by UVa presents has been performed. Results and comparison are presented in Appendix 9A.2.

[1] CIMEL scenario NLU is direct moon triplet (see deliverable D2 for further information)
[2] CIMEL scenario PLU is Polarized direct moon (see deliverable D2 for further information)

3.2 Traceability at NPL

3.2.1 Traceability to SI for irradiance at NPL

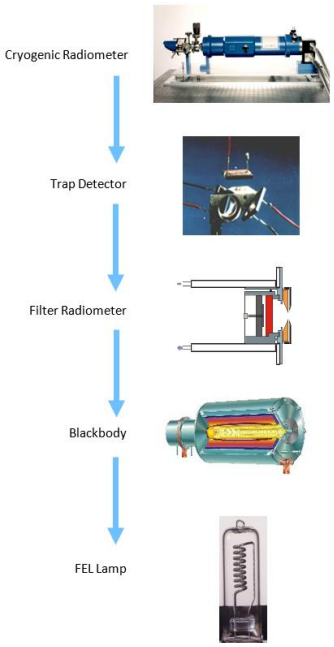

Figure 4: Traceability chain from the primary standard to an FEL lamp

Irradiance sources calibrated at NPL are traceable to the primary standard, the cryogenic radiometer. This works by comparing electrical power to optical power in a cryogenic blackbody cavity. The calibration is then transferred via a laser to a trap detector (an arrangement of Si photodiodes that reduce signal loss by reflectance to negligible levels). This in turn is used to calibrate a filter radiometer, which measures the radiance of a 3000 K blackbody source in the spectral band of the filter. From this, and Planck's Law, the temperature of the blackbody is known accurately, and hence the radiance at other temperatures. With an appropriate geometric system, consisting of two apertures, the radiance of the blackbody can be compared directly with the irradiance[3] of the FEL lamp at 500 mm from the reference frame, using a monochromator to measure each wavelength in turn. The FEL lamp is therefore a reference source of known spectral irradiance.

3.2.2 Traceability for a source at lunar irradiance levels

The irradiance source (the miner's lamp) that will be used for the MOON /SKY gain irradiance calibration (see section 7.4) cannot be calibrated directly against the blackbody because of its low power, and it does not maintain its calibration because it is not repeatable when re-aligned. Once switched on it is stable. For this reason a transfer spectrometer is used to transfer the calibration from the calibrated FEL lamp to the miner's lamp. This calibration will have to be done each time the system is switched on. It will also add an extra component of uncertainty into the final uncertainty budget.

3.2.3 Traceability for the CIMEL calibration

The CIMEL calibration described in this report is a combination of measurements directly against the FEL on the MOON gain, measurements against the Miner's lamp on the MOON gain and measurements against the FEL on AUR and SUN gains that have been corrected as though for MOON gain. A full description is given in

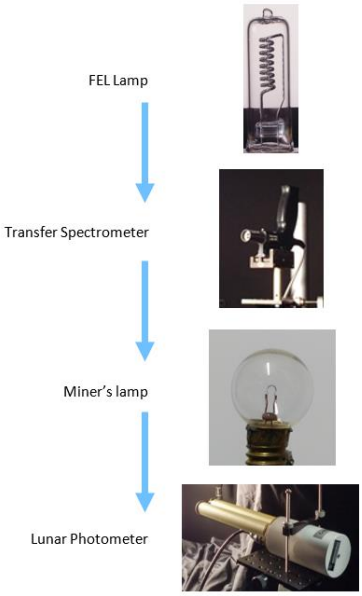

Figure 5: Extension of traceability chain to the lunar photometer

[3] The blackbody is a radiance source. A conversation to irradiance is made using two apertures (one in front of the blackbody and one in front of the monochromator system). The lamp is then measured as an irradiance source at a 500 mm distance from the monochromator system.

Section 7. These results assume that the instrument is linear, a test that is described in Section 5. The results have been corrected as though they were measured at 25 °C, as described in Section 4.

4 Temperature Characterisation

As the instrument is not thermally stabilised, the thermal sensitivity of the instrument must be determined. This is particularly important for 1020 nm, where Si is particularly temperature sensitive as it is approaching the bandgap, but is also necessary to determine for all spectral channels. It is therefore fundamental to perform a thermal characterisation of the instrument to compensate for the effect of the temperature variation during the realisation of day and night Langley plots. UVa has a thermal chamber suitable for these temperature sensitivity tests (operating from -30 °C to +50 °C).

4.1 Temperature statistics at the lunar photometer operation sites

The standard instrument operating temperature range of the photometer provided by the CIMEL Electronique is -30 °C to +40 °C (CIMEL, 2015).

Izaña	Jan	Feb	Mar	Apr	May	Jun	Jul	Aug	Sep	Oct	Nov	Dec
Temp. Max. [°C]	7.2	8.2	9.3	11.1	14.1	18.4	22.5	22.4	18.2	13.9	10.7	8.2
Temp. Min. [°C]	0.8	1.4	2.0	2.9	5.4	9.4	13.5	13.5	10.1	6.7	4.2	1.9

Table 1: Monthly mean of daily maximum and minimum temperatures at Izaña station

Table 1 shows the climatology of the maximum and minimum daily temperature by month for the Izaña station in the period 1971-2000. Table 3 shows the preliminary statistics from Pico Teide station, based on non-filtered data from 2013 to 2016

Pico Teide	Jan	Feb	Mar	Apr	May	Jun	Jul	Aug	Sep	Oct	Nov	Dec
Percentile 98 [°C]	7.7	8.0	8.7	11.7	14.1	16.6	18.7	18.8	15.1	13.0	9.9	7.5
Percentile 2 [°C]	-9.5	-12.0	-8.1	-5.7	-2.7	1.8	5.0	5.0	1.9	-3.5	-5.9	-8.2

Table 2: Monthly maximum and minimum temperatures at Pico Teide station

4.2 Temperature correction

A thermistor inside the CIMEL sensor head measures the temperature of the instrument. These temperature values, along with the temperature sensitivity characterization of the photometer in a temperature chamber, will allow compensation for any temperature dependence in the photometer measurements.

The irradiance, E_T measured in a temperature chamber at different temperatures T [°C], while the detector is illuminated with a stable light source, is fitted to the following model:

$$E_T = E_c + c'_1(T - T_{\mathrm{ref}}) + c'_2(T - T_{\mathrm{ref}})^2 \qquad \textit{Equation 2}$$

Where T_{ref} is the reference temperature (25 °C) and E_c is the irradiance of the source measured at the reference temperature.

When the lunar photometer is used at Teide Peak to measure the irradiance of the moon directly the (band integrated lunar) irradiance is given by

$$\overline{\boldsymbol{E}}_{\mathbf{moon}}(\boldsymbol{\lambda_i}) = [\boldsymbol{D}_{\mathbf{moon}}(\boldsymbol{\lambda_i}) - \boldsymbol{D}_{\mathbf{dark}}(\boldsymbol{\lambda_i})]\boldsymbol{C}_{\overline{E},\mathbf{CIMEL}}(\boldsymbol{\lambda_i})\boldsymbol{F_T} \qquad \textit{Equation 3}$$

Where

$$\boldsymbol{F_T} = \left[\mathbf{1} + \boldsymbol{C}_{\mathbf{1},i}(\boldsymbol{T} - \boldsymbol{T}_{\mathbf{ref}}) + \boldsymbol{C}_{\mathbf{2},i}(\boldsymbol{T} - \boldsymbol{T}_{\mathbf{ref}})^{\mathbf{2}}\right] \qquad \textit{Equation 4}$$

where $c_1 = c'_1/E_c$ [°C^{-1}]and $c_2 = c'_2/E_c$ [°C^{-2}].

The temperature factor F_T corrects for the difference in temperature between the reference calibration T_{ref} and the temperature during observation T. T is the temperature inside the photometer in degrees Celsius and $C_{1,i}$ and $C_{2,i}$ are temperature sensitivity coefficients determined for the photometer from temperature sensitivity checks.

The temperature corrections are applied to the raw data used to determine the spectral irradiance and radiance calibration coefficients determination at NPL (see sections 7 and **Error! Reference source not found.**)

4.3 Temperature sensitivity characterisation method

The temperature coefficients for the photometer are determined in a temperature chamber CLIMATS TM. It consists of a stainless steel cabinet with a gridding where the photometer can be positioned, and the right side has an 80 mm Ø hole. The photometer is aligned with an integrating sphere (Labsphere 10'' diameter), illuminated with a 100 W lamp, and powered by a stabilized power supply (Agilent E3634A). The stabilisation time for the integrating sphere is 20 minutes.

The temperature of the chamber is varied from 50 °C to -40 °C during a period of 4 hours, which is a rate of change of about 0.3 °C/min. The temperature ramp is started when instrument temperature reaches 40 °C. A typical measure of the signal level change for the 1020 nm channel is shown In Figure 7.

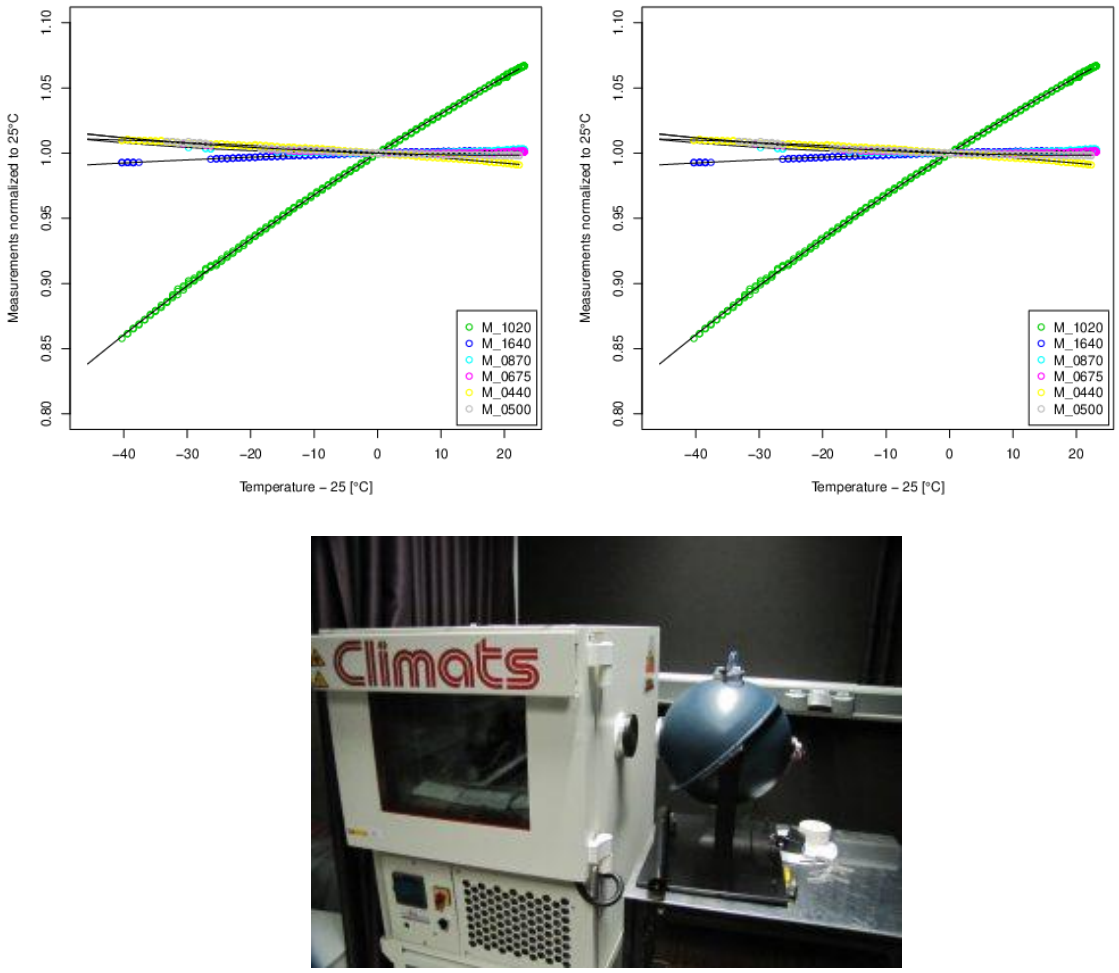

Figure 6: a) Temperature characterization December 2017, b) Temperature characterization January 2018, c) Temperature chamber and integrating sphere

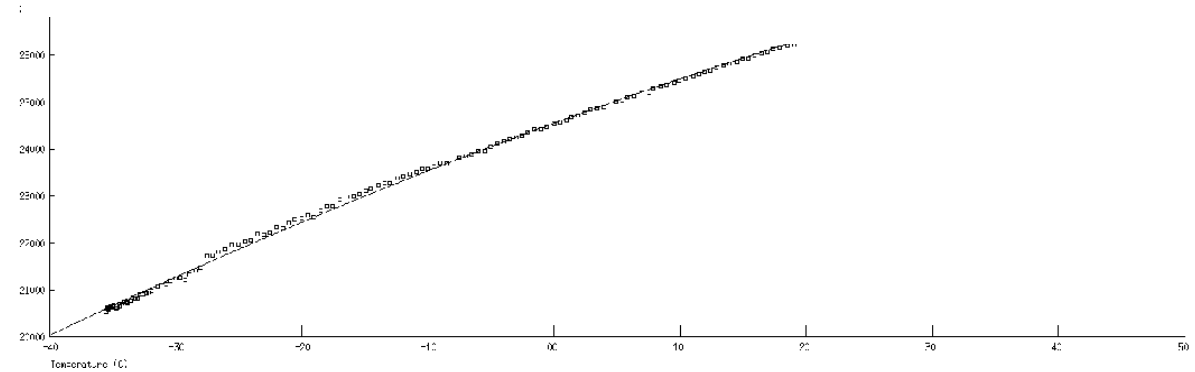

Figure 7: photometer signal level change with temperature – 1020 nm

4.4 Results

Two separate characterizations were carried out, in December 2017 and January 2018. The 1020 nm channel is, as expected, that most sensitive to temperature (Figure 7). While in December 2017

characterization only NLU[4] measurements were done in the thermal chamber, in January 2018 both NLU and PLU[5] measurements were done to characterise polarised channels as well. Temperature coefficients obtained by second order fitting and fitting uncertainties are shown in Table 3.

Dec2017(NLU)	c1	c2	u_c1	u_c2
M_1020	3.11E-03	-9.47E-06	3.15E-06	1.62E-07
M_1640	1.29E-04	-1.48E-06	1.09E-06	4.48E-08
M_0870	7.10E-06	5.12E-06	1.59E-06	1.00E-07
M_0675	-7.23E-05	5.49E-06	1.50E-06	9.62E-08
M_0440	-3.38E-04	-2.23E-06	1.62E-06	6.91E-08
M_0500	-1.53E-04	3.58E-06	1.66E-06	9.25E-08
Jan2018(NLU)	c1	c2	u_c1	u_c2
M_1020	3.02E-03	-9.12E-06	5.51E-06	2.46E-07
M_1640	1.33E-04	-1.03E-06	1.18E-06	6.15E-08
M_0870	-8.05E-05	8.16E-06	3.33E-06	2.19E-07
M_0675	-1.59E-04	8.27E-06	3.52E-06	2.21E-07
M_0440	-3.39E-04	5.37E-07	1.95E-06	9.40E-08
M_0500	-2.20E-04	6.95E-06	2.70E-06	1.52E-07
Jan2018(PLU)	c1	c2	u_c1	u_c2
M_1020	3.04E-03	-9.25E-06	1.00E-05	4.29E-07
M_1640	1.86E-04	-1.64E-06	2.24E-06	8.57E-08
M_0870	-8.03E-05	7.93E-06	6.54E-06	4.28E-07
M_0675	-1.63E-04	8.43E-06	6.11E-06	3.86E-07
M_0440	-3.37E-04	4.52E-08	5.27E-06	2.29E-07
M_0500	-2.14E-04	6.14E-06	5.69E-06	2.95E-07

Table 3: Coefficients obtained by second order fitting and standard errors

Table 4 provides uncertainties associated with the temperature coefficients as determined during the fit. In practice there will also be an error correlation between c1 and c2. To determine the uncertainty associated with the correction obtained from these coefficients, we estimate the difference between the temperature corrections associated with each set of coefficients for NLU measurements. This difference depends on the temperature, and is zero for the reference temperature (25°C). In order to provide example uncertainties, the difference between the correction calculated with each set of coefficients was determined at 11.3 °C as that is the mean temperature during Langley plots at Izaña observatory from June 2014 to October 2017.

	[%]
M_1020	0.13
M_1640	0.0027
M_0870	0.18
M_0675	0.17
M_0440	0.053
M_0500	0.15

Table 4: Estimate of uncertainty for the temperature correction at each filter central wavelength

Further discussion on the uncertainty associated to this temperature correction and its propagation is found in deliverable D4

[4] CIMEL scenario NLU is direct moon triplet (see deliverable D2 for further information)
[5] CIMEL scenario PLU is Polarized direct moon (see deliverable D2 for further information)

5 Linearity

5.1 NPL Linearity facility

For the CIMEL photometer to measure the moon and the sun, the instrument has a wide dynamic range. It is necessary to perform tests to ensure it has a linear response over this range. The most reliable method (and the method to be employed in the NPL linearity characterisation facility), is the double aperture method. This is based on the superposition principle. In this method the instrument is illuminated by two stimuli, first individually and then together. When the instrument is linear the signal with the two stimuli together should equal the sums of the signals with the two stimuli individually.

The NPL facility used a double aperture linearity wheel, and neutral density filters to vary the levels of radiation (see Figure 8 and Figure 9). The facility is fully automated, and allows the testing of the linear response of a detector over the range 200 nm to 20 µm (depending on the source used). The light emitted from the source (in this case a tungsten filament lamp) is first attenuated by initial filter wheel containing reflective neutral density filters. This filter wheel is positioned at an angle to incident radiation to avoid any inter reflections. The second wheel is the double aperture wheel, containing apertures A, B and A+B. The detector is mounted on a three-axis translation stage allowing the collimated beam to be accurately focused on the target channel.

A tungsten lamp is as the white light source, and filters will be used to allow us to measure the linearity across wavelength range 360 nm to 1640 nm.

The detector will be exposed to light first through aperture A, then aperture B, and then aperture equal to A+B. For a linear response we would expect the signal when both the apertures are open to equal the sum of the signal through each aperture individually. We can calculate a linearity factor $L(V_{\mathrm{A+B}})$

$$\boldsymbol{L(V_{A+B})} = \frac{\boldsymbol{V_{A+B}}}{\boldsymbol{(V_A + V_B)}} \qquad \textit{Equation 5}$$

Where V_{A} and V_{B} are the output signals when detector is illuminated by aperture A and B respectively (minus dark signal), and $V_{\mathrm{A+B}}$ is the dark subtracted output signal of the detector when illuminated by both A and B. A detection system is said to have a linear response when $L(V_{\mathrm{A+B}})$ is equal to unity (Theocharous, 2012).

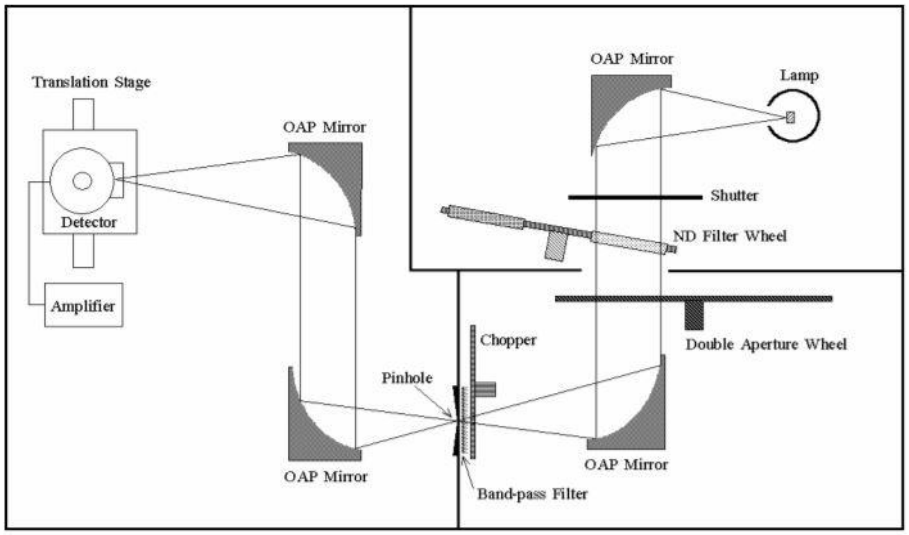

Figure 8: Schematic diagram of the layout of the NPL linearity facility. OAP: off axis parabola. ND: neutral density [Theocharous, 2011]

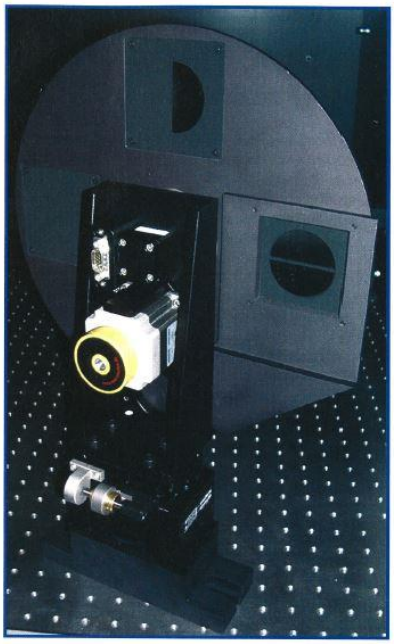

Figure 9: The double aperture wheel at the NPL linearity response measurement facility [Theocharous, 2007]

5.2 Results

The linearity results are shown in the figures below. The table provides the average linearity measurements. For 340 nm and 380 nm there was not enough signal to get a meaningful estimates of the linearity. We would anticipate the true linearity in these channels to be similar to those of other spectral channels as the main source of nonlinearity is the detector.

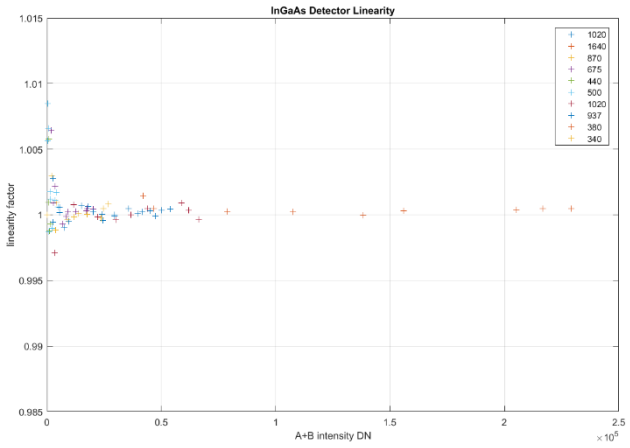

Figure 10: Linearity results for InGaAs detector on MOON gain

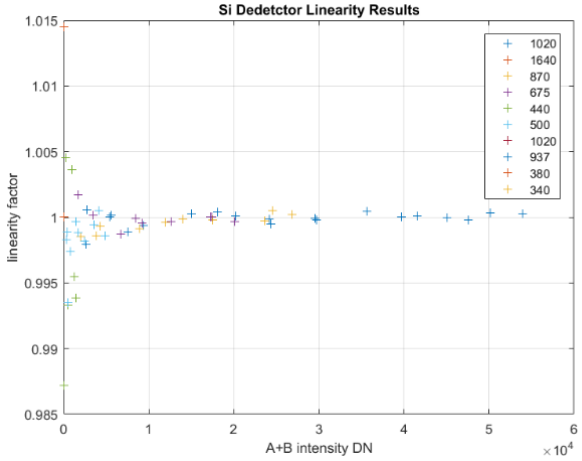

Figure 12: Linearity results for SI detector on MOON gain

Filter transmission	340	380	440	500	675	870	937	1020	1020i	1640
100 %	0.5532	0.9121	0.9938	0.9986	0.9997	1.0002	1	1.0003	0.9971	1.0015
56 %	1.3333	0	1	0.9981	0.9997	0.9998	0.9999	1.0004	1.0009	1.0004
28 %	0	0	1	0.9989	1.0005	0.9993	0.9989	0.9994	0.9996	1.0002
12 %	0.6364	0.88	1.0037	0.9994	1	1.0005	1.0001	1.0003	1.0003	1.0005
33 %	0	0.8571	1	0.9935	0.9999	0.9996	1.0001	0.9995		1.0005
91 %	0.7	1.0145	0.9933	0.9988	0.9987	0.9991	1.0003	1.0004	1.0008	1.0003
87 %	0.6923	1.0625	0.9955	1.0005	1	0.9997	1	0.9998	1	1
10 %	0.1667	0.8	0.9872	0.9983	1.0017	0.9985	1.0006	0.9979	1.0005	1.0003
21 %	0.3333	1	1.0045	0.9974	1.0001	0.9986	1	1.0002	0.9996	1.0005
Ave	0.490578	0.725133	0.997556	0.998167	1.000033	0.999478	0.999989	0.9998	0.9998	1.00048
Stdev	37.83%	37.51%	0.50%	0.18%	0.07%	0.06%	0.04%	0.07%	0.11%	0.04%

Table 5: Linearity results for MOON gain, SI detector for varying illuminations, average and standard deviation

Table 6 presents the results of the linearity characterisation. Linearity is calculated for illumination levels varied by changing the neutral density filters, we then average the results for the final estimation of linearity for each CIMEL spectral channel. For wavelengths of 500 nm and beyond, the nonlinearity is less than 0.1 % with a standard deviation of values for different levels of less than 0.1 % and the graphs (Figures 11 and 12) show no systematic pattern. Therefore here nonlinearity is considered negligible.

At shorter wavelengths the variability is considerable, but shows no pattern. Here too we assume nonlinearity (which is predominantly a detector phenomenon and therefore common between wavelengths) is negligible and this variability is due to measurement noise for low signals.

6 Determination of Reference Planes

6.1 The need for a reference plane

The irradiance calibration coefficients are measured against sources at several finite distances. When the instrument is used to measure the moon and sun, these are, of course, at very much greater distances (effectively infinity). To perform an accurate calibration of irradiance, the irradiance of the source at the distance of measurement must be known.

The well-known inverse square law provides a means to correct for distance, but it is only applicable when the sources are point sources and the distance to the detector is well defined. Real sources have finite filaments and often a defining plane that is offset from the centre of that filament. Similarly, the detector is embedded within the CIMEL photometer and the distance to the defining aperture of the detector system is different to that which makes a convenient reference plane.

In order to account for this we needed to determine the offset distance for the FEL lamp used as a calibration reference, and for the CIMEL photometer.

6.2 FEL filament offset

The distance offset of the FEL lamps used in the irradiance responsivity characterisation need to be quantified as the FEL lamp will be used at distances other than the calibration distance of 500 mm.

To establish this offset distance in the absence of other effects, the NPL reference photometer[6] was used as the reference detector. This has a high precision aperture at the front, providing a clear reference plane and therefore has no offset distance of its own.

The irradiance of a lamp is given by the following equation (Manninen. P., 2006)

$$\boldsymbol{E(D)} = \frac{\boldsymbol{I}}{\boldsymbol{(D+f)^2 + r_f^2 + r_d^2}} \qquad \textit{Equation 6}$$

where I is the radiant intensity (W sr^{-1}), D is the distance between the lamp's reference plane and detector, f is the filament offset distance for the lamp, r_f is the filament size, r_d is the detector size.

We assume that for sufficiently large distances, r_f and r_d are negligible. If $r_f < 0.03 \times D$, then the effect of ignoring it is <0.1 %.

Measurements of the FEL with the NPL reference photometer were taken at distances ranging from 2000 mm to 4500 mm. The bulb of an FEL lamp is approximately 50 mm in its largest dimension. This is less than 3 % of the smallest distance, therefore a simplified modified inverse square law can be used. Here we take a ratio to the shortest distance, thus:

$$\boldsymbol{K} = \frac{\boldsymbol{V(D)}}{\boldsymbol{V(D_{\text{ref}})}} = \left(\frac{\boldsymbol{D_{\text{ref}} + f}}{\boldsymbol{D + f}}\right)^{\boldsymbol{2}} \qquad \textit{Equation 7}$$

[6] Here "photometer" is used in its true sense as a radiometer whose spectral response function mimics the human eye response.

Where, K is the signal ratio, $V(D)$ is the signal with a measured distance $D$and $V(D_{\text{ref}})$ is the signal with the reference distance D_{ref}. This must be equal to the inverse of the squares of the full distances given by the measured distances and the filament offset distance f.

In order to estimate the filament offset distance in the simplest way, we rearrange this equation to get

$$\boldsymbol{D\sqrt{K} - D_{\text{ref}} = f\left(1 - \sqrt{K}\right)} \qquad \textit{Equation 8}$$

Thus, by plotting a graph of $D\sqrt{K} - D_{\text{ref}}$ against $\left(1 - \sqrt{K}\right)$ we expect a straight line, through the origin, with a slope f. The result is shown in Figure 12.

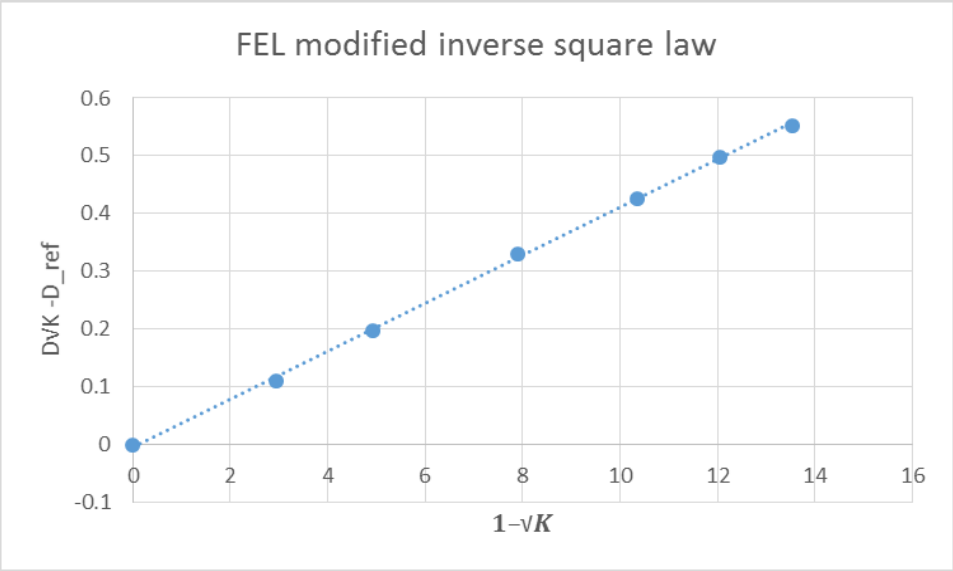

Figure 12 Straight line for the FEL

From the slope of this graph, the distance offset for the FEL 399 was calculated to be *d* = 24.52 mm. This is a reasonable value for an FEL lamp, which is aligned to a front plate and not the filament.

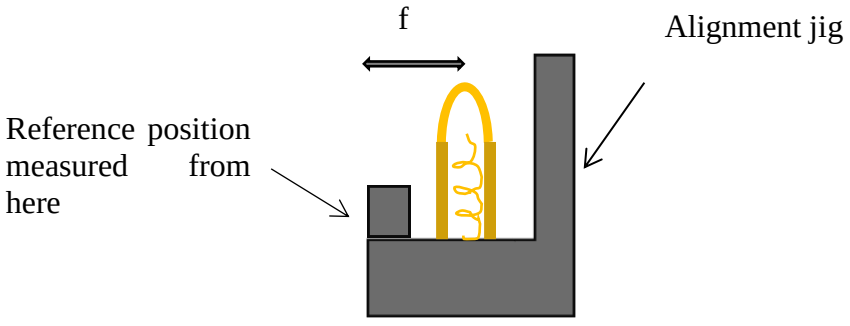

Figure 13: Schematic of the FEL lamp mount with the reference position on the left part and the jig on the right side. The distance offset is indicated as f

Because of the high degree of correlation between the x and y axes in this graph (both are based on the same data) we do not perform uncertainty analysis with respect to the fit in the way that would be used in ordinary fitting uncertainty analysis. Instead we estimated the uncertainty by considering other "reasonable" (by eye) lines through the measured points. An uncertainty of 0.5 mm was assigned to f .

The relative irradiance uncertainty due to distance offset uncertainty is

$$\left[\left(\frac{2u(d)}{D+d}\right)^2+\left(\frac{2u(d)}{500+d}\right)^2\right]^{1/2}[\%] \qquad \textit{Equation 9}$$

Distance (D)	Filament offset uncertainty $u(f)$ mm	Relative irradiance uncertainty due to distance offset uncertainty
500	0.5	0.27%
1000	0.5	0.21%
1500	0.5	0.20%
2000	0.5	0.20%
2500	0.5	0.19%
3000	0.5	0.19%
3500	0.5	0.19%
4000	0.5	0.19%
4500	0.5	0.19%
5000	0.5	0.19%

Table 6: Irradiance uncertainty due to FEL filament offset uncertainty

6.3 Distance offset of SI and InGaAs Detectors in CIMEL photometer

In order to measure the offset distance for the CIMEL photometer, we performed an analysis with a Polaron lamp. The Polaron lamp was chosen because it has a relatively small offset distance of its own. Unlike an FEL it is not aligned to an external reference plane, but to the filament itself. This is done by looking at the filament with a telescope that is set at a particular distance.

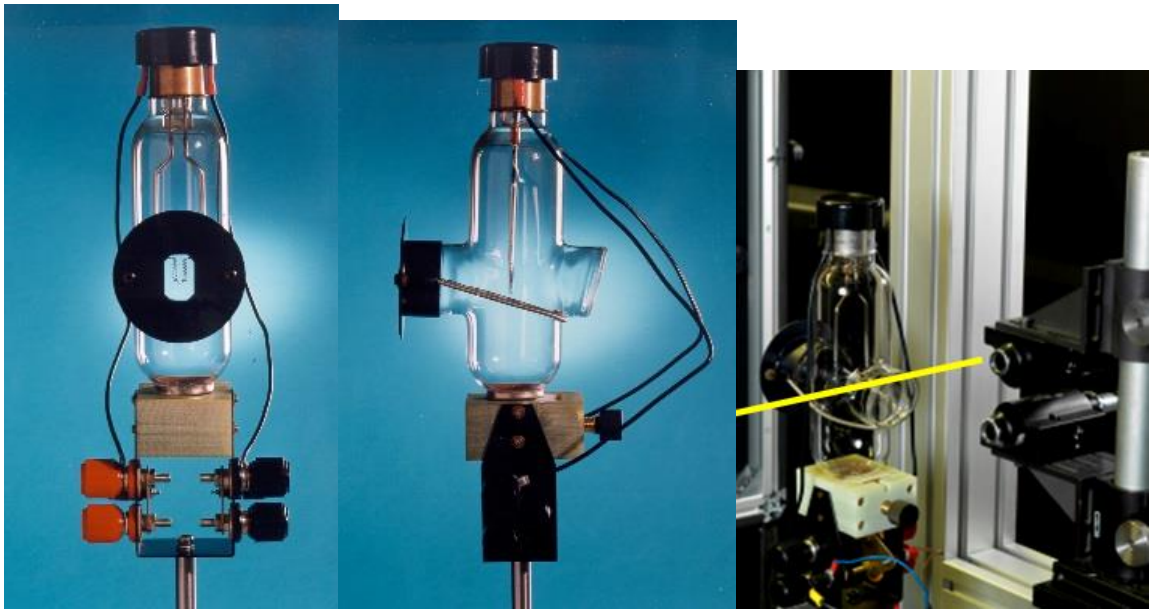

Figure 14A Polaron lamp and its alignment methodology

The Polaron lamp offset distance was calculated to be -2.3 mm by one calibration and -2.58 mm in an independent calibration. We expect this distance to be partly due to the glass envelope (effective distance extension due to refraction) and partly due to the filament physical dimensions.

The CIMEL was aligned to a convenient reference plane at the back of the instrument. We anticipated a large distance offset to the true measurement point of the instrument. Equation 7 becomes

$$\boldsymbol{K = \frac{V(D)}{V(D_{\text{ref}})} = \left(\frac{D_{\text{ref}} + f + d}{D + f + d}\right)^2} \qquad \textit{Equation 10}$$

where f is the (now known) Polaron filament offset distance and d is the CIMEL detector offset distance. We can similarly rearrange this to get:

$$\boldsymbol{(D + f)\sqrt{K} - (D_{\text{ref}} + f) = d\left(1 - \sqrt{K}\right)} \qquad \textit{Equation 11}$$

This distance calculation was performed before the CIMEL calibration and offset distances of -129.9 mm for the Si detector channels and -138.1 mm for the InGaAs channels were determined. These distances were used in the laboratory; that is the FEL-CIMEL and miner's lamp – CIMEL distances were physically set by subtracting this distance from the known distances.

6.4 Validating the distance offset for the CIMEL

The CIMEL distance offsets were determined prior to the irradiance coefficient calibration of the CIMEL using this Polaron data. However, several measurements had to be removed from analysis as the signal did not follow the straight line expected for short distances (because of the lamp size?) and some data points suffered from stray light. Therefore it was important to validate this distance correction. Since both the FEL and Miner's lamp calibrations were performed at several different distances, we have a mechanism for independently validating the calculated offset distances.

In the figures below we show the calibration coefficients obtained using the FEL lamp at different nominal distances. Full details are described in sections below. In the first graph these are the results

based on the distance set in the lab (takes into consideration the assumed CIMEL offset distance) and a post-correction for the FEL filament distance.

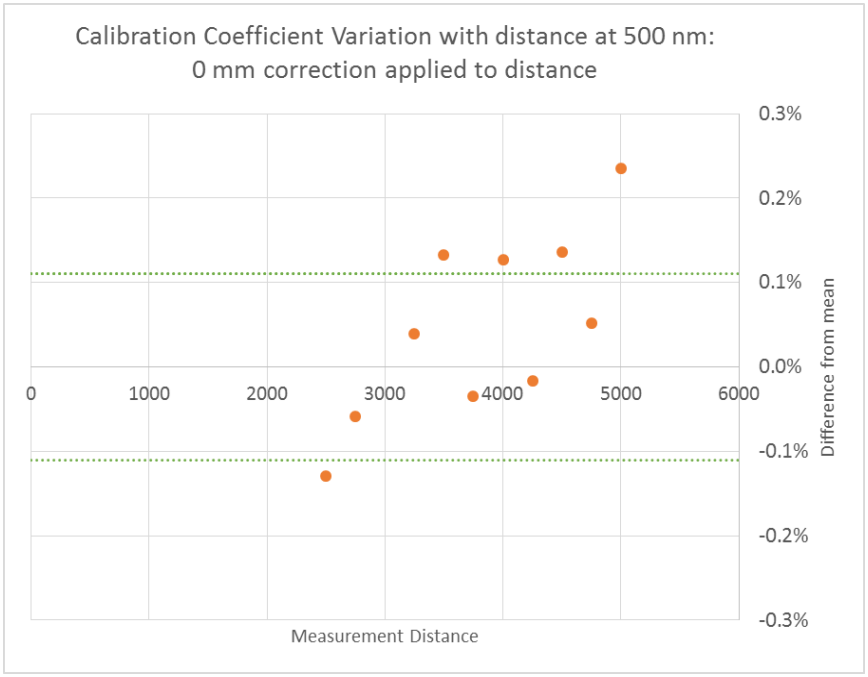

Figure 15

The second graph shows results when the offset was assumed to be wrong by +2.5 mm and a post-correction was applied.

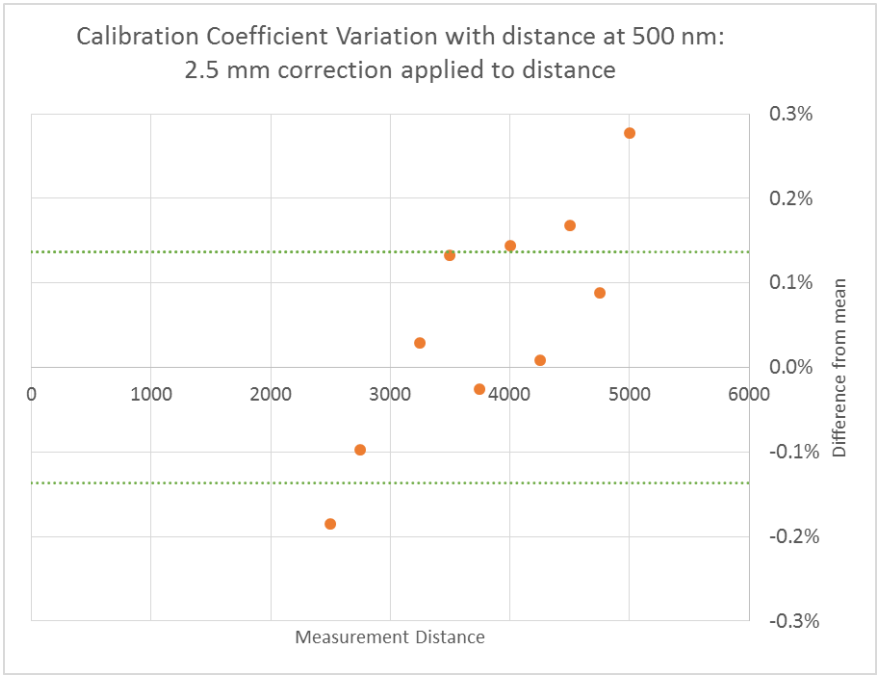

Figure 16

The third graph shows the results when the offset was assumed to be wrong by -2.5 mm and a post-correction was applied.

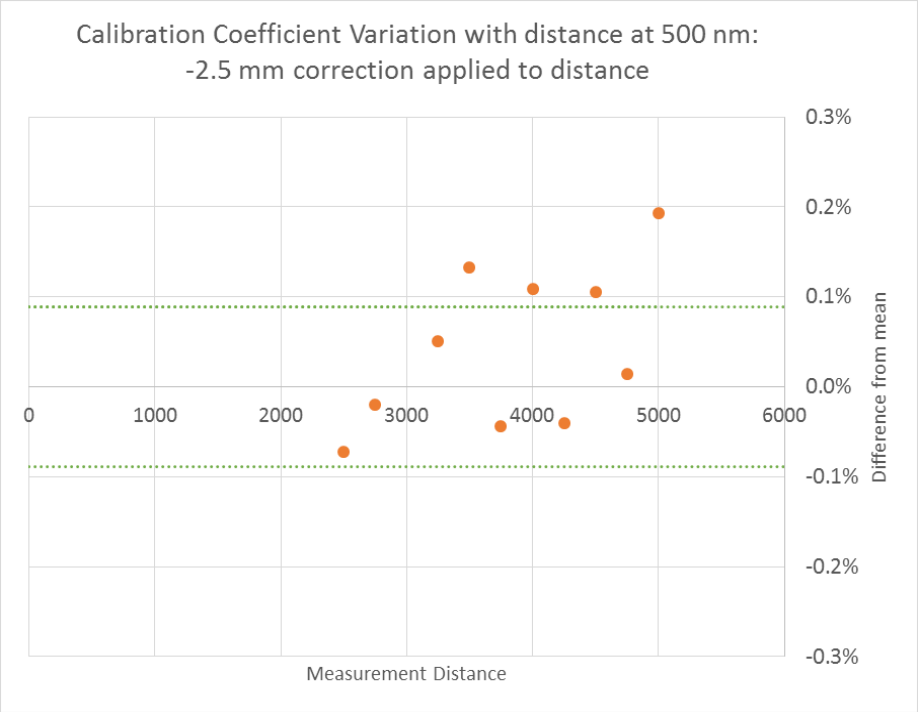

Figure 17

It is clear that reducing the distance by this small amount improves the agreement between different measurement distances, while increasing the distance worsens that agreement.

This analysis was repeated for all wavelengths and for both the AUR and SUN gain calibrations with the FEL, as well as for the MOON gain calibrations for the miner's lamp. We plotted the relative standard distribution of the results at different distances (the green dotted lines in the graphs above) as a function of correction distance for each channel.

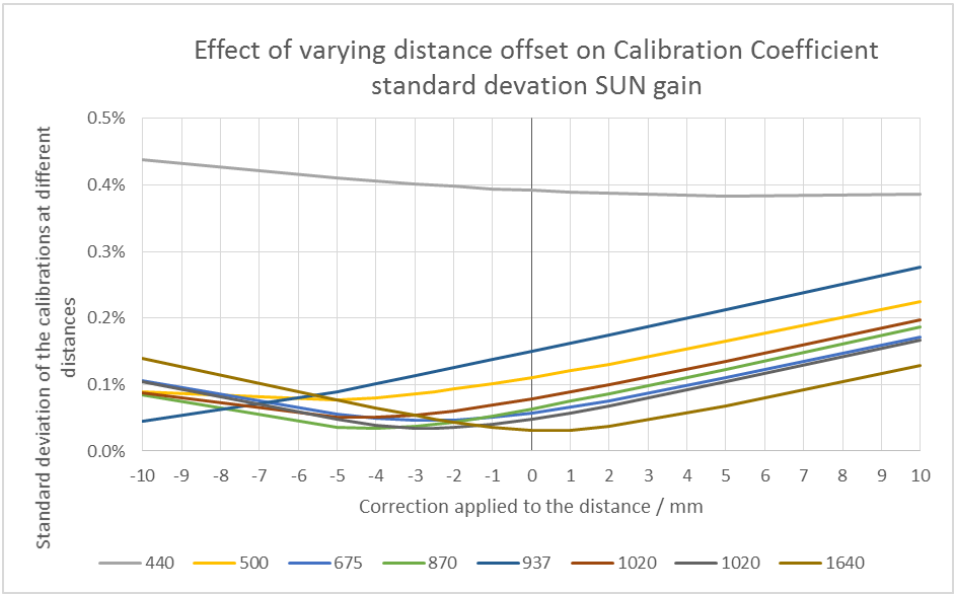

Figure 18 Variation in the standard deviation of the calibration coefficients for different distances (green dotted line in previous figures) as a function of the distance correction applied, for the SUN gain measurements with an FEL

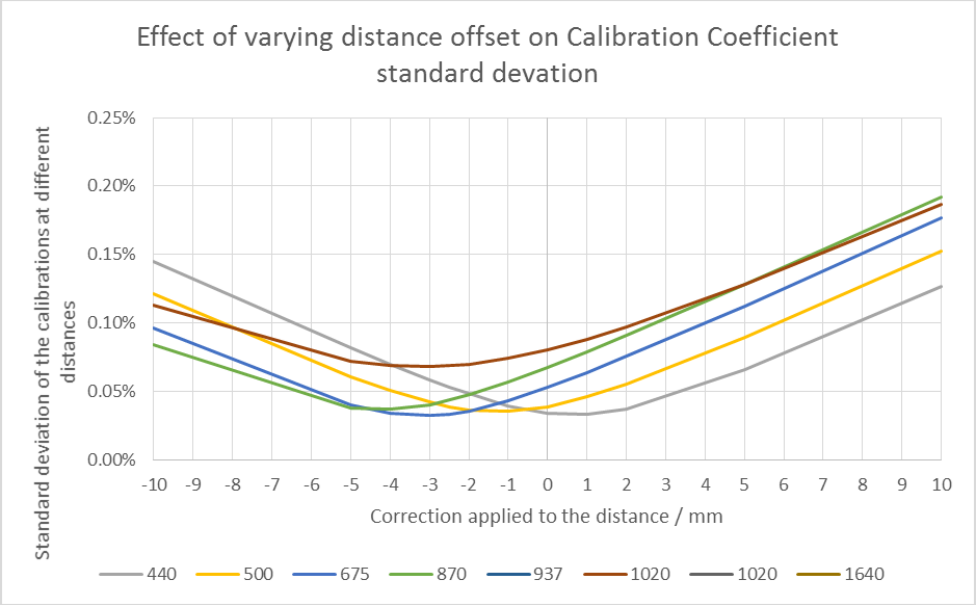

Figure 19 Variation in the standard deviation of the calibration coefficients for different distances (green dotted line in previous figures) as a function of the distance correction applied, for the AUR gain measurements with an FEL

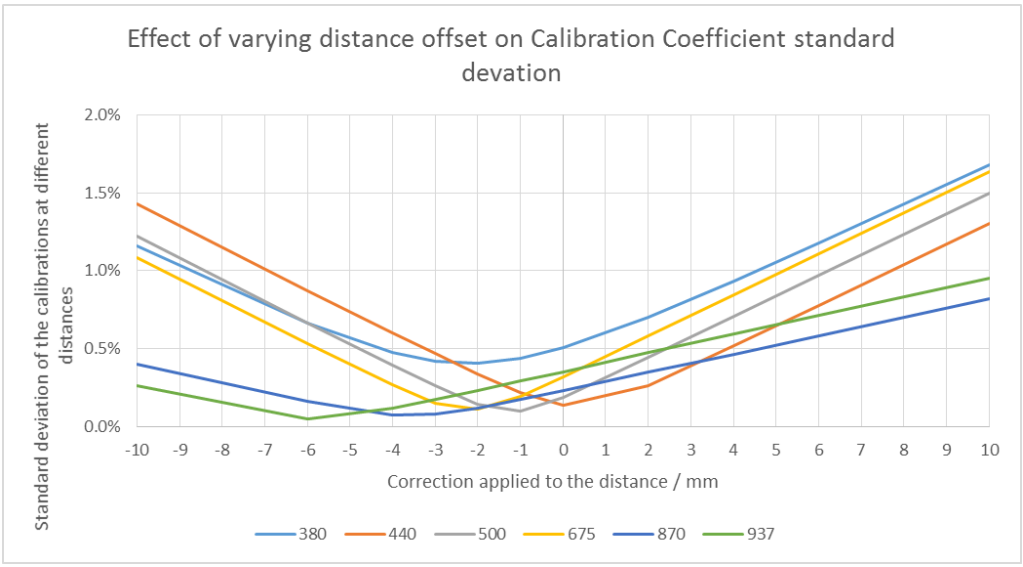

Figure 20Variation in the standard deviation of the calibration coefficients for different distances (green dotted line in previous figures) as a function of the distance correction applied, for the MOON gain measurements with a miner's lamp

The results show some variability, though the inter-channel differences are not consistent for the three sets of measurements.

Reviewing all the data, we chose to include a -2.5 mm correction on the distance as a reasonable approximation, with a 2.5 mm uncertainty associated with that correction. This is considered the error in the determination of the CIMEL offset distance (which was set physically in the laboratory) based on the Polaron measurements (and is applied to all channels and both miner's lamp and FEL measurements). It is worth noting that the Polaron offset distance was calculated as approximately -2.5 mm and it is possible that this was not included in the CIMEL distance measurements. If that is the case we have independently verified both the Polaron offset distance and that the determined CIMEL offset distance is correct.

The distance uncertainty of 2.5 mm feeds into a radiometric uncertainty of approx. 0.8 % for the FEL (minor variations with distance and detector; see D4). The residual spread (standard deviation shown above) is included as a "noise" effect in the uncertainty analysis (see D4).

7 Irradiance Responsivity

7.1 Background / considerations / assumptions

Irradiance responsivity is most accurately measured using a point source and a detector with a defined area and very large field of view (for example an integrating sphere or transmissive diffuser, but a simple filter detector with a single aperture can also be used). A larger source can be used, but it must fit within the angular field of view of the detector, otherwise light from the source that should be measured will be lost.

The lunar photometer used in this study is a development of an earlier model of the instrument only used to measure the irradiance of the sun. Measuring the irradiance of the sun is challenging because a simple irradiance instrument, with a typically large field of view, would measure both the irradiance of the sun and the irradiance of the sky. To prevent this, a lens is attached, which limits the field of view to 1.3° (plane angle). A collimator is attached to reduce the straylight (section 2.2.1). Measurements of the sun and moon using the lunar photometer are irradiance measurements i.e. the photometer is collecting all the light from the source that hits its detector area. The apertures that define the field of view here only act to cut out some stray light.

The angular diameter of the moon is between 29.94 arc minutes and 33.66 arc minutes and the sun is approximately 32 arc minutes. They are both therefore around half a degree across, fitting within the 1.3° diameter field of view of the lunar photometer. The contribution of diffuse radiation into the field of view during daytime at this high altitude stations is negligible due to the very low aerosol optical depth (see Toledano et al., 2018 and references therein). During nightime the sky does not contribute to the direct moon signal (it is dark for the instrument sensitivity).

We therefore need to use irradiance lamps that fit entirely within the FOV of the lunar photometer, and provide enough signal, without saturation.

As shown in the traceability chain of Section 0, the typical spectral irradiance source at NPL is the Gigahertz BN-9101 FEL 1000 W lamp, which has a filament of about 1 cm × 4 cm and is calibrated at 500 mm distance. If the CIMEL photometer (nominal FOV 1.3 degrees) was placed at 500 mm from the lamp the area it views is just over a centimetre. The distance it would have to be at to see all of the filament is greater than 2.2 metres, which would reduce the signal level by about 20 times, sufficient for the SUN and AUR gain, and for some of the filters within the SKY scenario, however it saturates the MOON gain for all but the shortest wavelengths.

To supplement the FEL calibration, we also used a miner's lamp. This lamp is tiny, with a filament only a few millimetres in size, and the envelope of the bulb around 2 cm. The filament will therefore be within the photometer field of view if the CIMEL and the lamp are more than 1 m apart. The power of the lamp is around 1 W, which provides a very low irradiance level suitable for MOON gain calibrations. Unfortunately it is not a calibrated lamp, which means we will need to transfer the calibration from a brighter calibrated lamp using a transfer spectrometer (an ASD FieldSpec).

7.2 Overview of the irradiance calibration process

The CIMEL photometer calibration for band-integrated irradiance calibration coefficients for MOON gain was determined in four ways:

- A direct calibration against an FEL lamp (FEL399)
- A calibration against a miner's lamp which was itself calibrated against an FEL lamp (FEL401) using an ASD as a transfer instrument
- A calibration against an FEL lamp (FEL399) on the SUN gain, and a correction for the MOON gain using the known gain ratios.
- A calibration against an FEL lamp (FEL399) on the AUR gain, and a correction for the MOON gain using the known gain ratios.

For some wavelengths one or more of these methods was not possible because the signal was either too low or too high to be measured. A table of methods for each spectral channel is given in Table 7

Spectral Channel	Direct FEL	Miner's Lamp Calibration	SUN/MOON ratio	AUR/MOON ratio
340 nm Si	4 m and 5 m		2.5 m to 5 m	2.5 m to 5 m
380 nm Si	4 m and 5 m	0.5 m and 1 m	2.5 m to 5 m	2.5 m to 5 m
440 nm Si	4 m and 5 m	0.5 m to 3 m	2.5 m to 5 m	2.5 m to 5 m
500 nm Si	5 m	0.5 m to 3 m	2.5 m to 5 m	2.5 m to 5 m
675 nm Si		0.5 m to 3 m	2.5 m to 5 m	2.5 m to 5 m
870 nm Si		1 m to 3 m	2.5 m to 5 m	2.5 m to 5 m
937 nm Si		1 m to 3 m	2.5 m to 5 m	
1020 nm Si			2.5 m to 5 m	2.5 m to 5 m
1020 nm InGaAs			2.5 m to 5 m	
1640 nm InGaAs			2.5 m to 5 m	2.5 m to 5 m

Table 7: Methods for determining calibration coefficients for the MOON gain for each spectral channel

7.2.1 Generic measurement function

The generic measurement function for all methods is

$$C_{\bar{E},\mathrm{CIMEL}}(\lambda_i) = \frac{\left(\sum_j E_{\mathrm{lamp},x}(\lambda_j)\xi_i(\lambda_j)\delta\lambda\right)F_T}{G_{\mathrm{ratio}}\left[D_{\mathrm{CIMEL,lamp},x}(\lambda_i) - D_{\mathrm{CIMEL,dark}}(\lambda_i)\right]} + 0 \qquad \textit{Equation 12}$$

where

$C_{\bar{E},\mathrm{CIMEL}}(\lambda_i)$	**Is the band-integrated irradiance calibration coefficient for band i of the CIMEL at wavelength λ_i**
$E_{\mathrm{lamp},x}(\lambda_j)$	Is the irradiance of the lamp at wavelength λ_j and distance x See below
$\xi_i(\lambda_j)$	Is the normalised (for unit area) spectral response function at wavelength λ_j defined at equi-spaced wavelengths λ_j separated by $\delta\lambda$
F_T	Is the temperature correction from the calibration instrument temperature to the nominal reference temperature of 25 °C
G_{ratio}	Is the gain ratio from the gain of measurement (e.g. SUN or AUR) to the MOON gain $4096 = \frac{C_{\mathrm{SUN}}}{C_{\mathrm{MOON}}}$ and $32 = \frac{C_{\mathrm{AUR}}}{C_{\mathrm{MOON}}}$

$\boldsymbol{D_{\mathrm{CIMEL,lamp},x}(\lambda_i)}$	Is the CIMEL signal for channel at wavelength λ_i when looking at the lamp at distance x
$\boldsymbol{D_{\mathrm{CIMEL,dark}}(\lambda_i)}$	Is the dark signal for channel at wavelength λ_i
$\mathbf{0}$	Represents the approximations in the form of the equation, in particular that the CIMEL is linear and that the summation on the numerator is an appropriate approximation for the spectral integral. (Included for uncertainty analysis and discussed in D4; to obtain the calibration coefficients this takes the value of 0)

The irradiance of the lamp at distance x is given as discussed above by

$$E_{\mathrm{lamp},x}(\lambda_j) = E_{\mathrm{lamp,cal}}(\lambda_j)\frac{(x+d+f)^2}{(x_{\mathrm{ref}}+d+f)^2} + 0 \qquad \textit{Equation 13}$$

Where

$E_{\mathrm{lamp,cal}}(\lambda_j)$	Is the irradiance of the lamp at its calibration distance
$x+d$	Is the measurement distance. In the lab we corrected for the CIMEL offset distances, as discussed in Section 6.3
f	Is the filament offset distance for the lamp
0	Is there for uncertainty analysis and acknowledges that we have ignored effects relating to the physical size of the filament and detector.

7.3 SUN and AUR gain irradiance characterisation using FEL lamp

For spectral irradiance calibration of the SUN and AUR gain and for a few wavelengths on SKY and MOON gains, a FEL lamp can be used directly to derive the band-integrated irradiance calibration coefficient for the CIMEL. Here Equation 12 can be used directly, where the lamp is an FEL with the filament offset distance of 24.52 mm (See section 6.2).

In equation 7-1 the integral $\int E_{\mathrm{FEL}}(\lambda)\xi_i(\lambda)\mathrm{d}\lambda$ has been replaced by the discretised sum: $\sum_j E_{\mathrm{FEL}}(\lambda_j)\xi_i(\lambda_j)\delta\lambda$. This is the trapezium rule assumption, considering equispaced data[7], and the difference between the integral and the sum is assumed to be very close to zero. The spectral step size is taken to be 0.1 nm, the step size the relative SRF has been provided in. The (smoothly varying) lamp spectral irradiance has been interpolated to these wavelengths[8]. Different interpolation approaches were compared, including simple splines. The method used was a standard approach for interpolating a tungsten-based lamp. Tungsten lamps emit light because they are hot, and therefore have spectra dominated by the blackbody spectrum (particularly for double-coiled filament lamps like

[7] For a trapezium rule with equispaced data the first and last step should be multiplied by $\delta\lambda/2$ and intermediate steps by $\delta\lambda$, but given that the spectral response function falls off to zero at both ends, the effect of ignoring this is extremely small (and probably less than other approximations in the trapezium rule).

[8] A comparison was made with different interpolation methods, including a spline fit and dividing the spectral irradiance with the best fit Planck curve (fit to temperature) and then interpolating the result before remultiplying by the Planck curve.

the FEL). If the measured irradiance is divided by an appropriate blackbody curve, the resultant spectral shape comes from a mixture of tungsten emissivity and glass transmittance and is smoothly varying. This can either be interpolated using a spline fit, or smoothed using a high order (12th-14th) polynomial fitted to the irradiance values. The interpolated or fitted residual shape is then remultiplied by the blackbody curve to obtain the original lamp irradiance.

7.3.1 Measurements

Measurements were acquired in the NPL 8 m bench lab for distances ranging from 2500 mm to 5000 mm, using FEL lamp 399 and for two repeats on both SI and InGaAs detectors. Previous measurements with a Polaron lamp indicated that the SUN gain setting would produce results at a meaningful signal level. The SKY/MOON gain setting was expected to saturate on some channels. Measurements were taken with SUN and SKY scenarios at every distance, and MOON scenario at selected distances. Two sets were done, one with measurements from 2500 mm to 5000 mm, every 250 mm. The second set included measurements at 2500 mm, 3000 mm and 3500 mm only.

The distance offset of the SI and InGaAs detectors (calculated in section 6) were included in the distance setting calculations during laboratory calibration. The uncertainty associated with these values is also included in the combined uncertainty.

Further discussion of the uncertainty associated with these calibration coefficients can be found in project deliverable D4, section 3.4.1.

7.3.2 Results

	SUN		AUR		MOON	
	Cal coeff	*k*=1 unc / %	Cal coeff	*k*=1 unc / %	Cal coeff	*k*=1 unc / %
340	2.143E-05	10.86%	1.69064E-07	1.43%	5.33E-09	1.40%
380	9.032E-06	3.18%	7.12916E-08	1.24%	2.25E-09	1.24%
440	2.383E-06	1.16%	1.84693E-08	1.06%	5.82E-10	1.06%
500	1.856E-06	1.04%	1.43649E-08	1.02%	4.53E-10	1.02%
675	1.331E-06	1.00%	1.03213E-08	0.99%		
870	1.051E-06	0.98%	8.14391E-09	0.97%		
937	9.982E-07	1.00%				
1020	1.130E-06	1.02%	8.75096E-09	1.00%		
1020 (InGaAs)	8.752E-07	1.01%				
1640 (InGaAs)	2.022E-07	1.02%	1.56502E-09			

Table 8: Irradiance calibration coefficients determined from direct FEL calibration (September 2018 temperature correction)

7.4 SKY & MOON gain irradiance characterisation using Miner's lamp and ASD

7.4.1 Lunar Irradiance from FEL-ASD-Miner's Lamp

To obtain spectral irradiance calibration coefficients directly for the MOON gain, we used the miner's lamp. As this lamp is not sufficiently stable to hold a calibration, it was calibrated each time it was used with an ASD with an irradiance input optic, which had in turn been calibrated against the FEL at the FEL –calibration distance.

7.4.1.1 Step 1: ASD measurements of calibrated FEL lamps

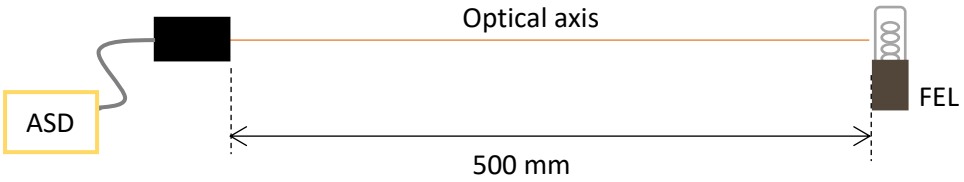

Figure 21: ASD measurement set up for transfer of calibration from FEL to miner's lamp

The transfer spectrometer is set up at the calibration distance of the FEL lamp and the ASD measurements of the spectral irradiance of the FEL are used to determine calibration coefficients for the ASD.

The measurement function for the calibration of the ASD against the FEL is given by:

$$C_{E,\mathrm{ASD}}(\lambda) = \frac{E_{\mathrm{FEL}}(\lambda)}{D_{\mathrm{ASD,FEL}}(\lambda) - D_{\mathrm{ASD,dark}}(\lambda)} \qquad \textit{Equation 14}$$

where $C_{E,\mathrm{ASD}}(\lambda)$ is the spectral irradiance calibration coefficient [units W m^{-2} nm^{-1} count^{-1}] of the ASD for the spectral channel λ, $E_{\mathrm{FEL}}(\lambda)$ is the irradiance of the FEL at this wavelength [W m^{-2} nm^{-1}], $D_{\mathrm{ASD,FEL}}(\lambda)$ is the count signal at this spectral channel when observing the FEL and $D_{\mathrm{ASD,dark}}(\lambda)$ is the dark count signal. These measured counts are corrected for the integration time of the instrument.

Note that this calibration was performed at each ASD wavelength. AS the FEL lamp had been calibrated in 10 nm steps, it needed interpolating spectrally, as described above.

7.4.1.2 Step 2: ASD measurements to determine miner's lamp irradiance

The calibrated FEL lamp is then replaced by the miner's lamp and the transfer spectrometer left in position. The irradiance of the miner's lamp then measured by the transfer spectrometer.

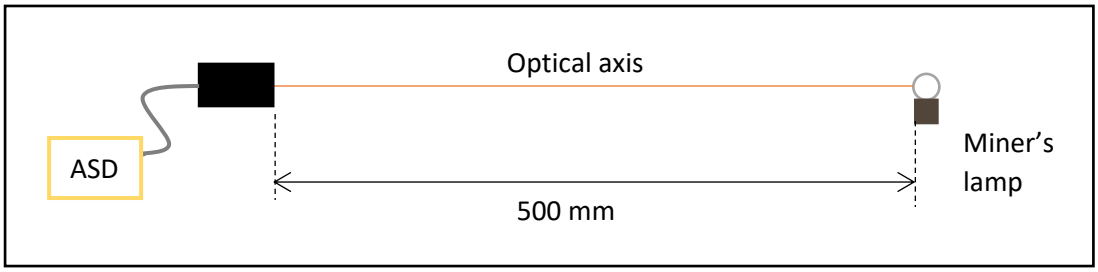

Figure 22: Diagram of set up of ASD measurements of miner's lamp.

The irradiance of the miner's lamp, as measured by the ASD is given by

$$E_{\mathrm{miner}}(\lambda) = \left[D_{\mathrm{ASD,miner}}(\lambda)\right] C_{E,\mathrm{ASD}}(\lambda) \qquad \textit{Equation 15}$$

7.4.1.3 Step 3: CIMEL C_{MOON} from E_{ML}

The transfer spectrometer is replaced by the CIMEL photometer, leaving the miner's lamp powered and maintaining its alignment so that the calibration transfer remains valid. Measurements taken on MOON and SKY gain at distances varying from 500 mm – 3000 mm (the CIMEL was moved so the miner's lamp was untouched). The CIMEL calibration offset distance was used in the laboratory as a physical offset.

While the ASD makes measurements in narrow spectral bands[9], the CIMEL lunar radiometer makes measurement in spectral bands. Thus the band-integrated irradiance calibration coefficient of the CIMEL for spectral band, λ_i , is given by

$$C_{\bar{E},\mathrm{CIMEL}}(\lambda_i) = \frac{\left(\sum_j E_{\mathrm{miner}}(\lambda_j)\xi_i(\lambda_j)\delta\lambda\right)F_T}{\left[D_{\mathrm{CIMEL,miner}}(\lambda_i) - D_{\mathrm{CIMEL,dark}}(\lambda_i)\right]} \qquad \textit{Equation 16}$$

Where $\xi_i(\lambda_j)$ is the CIMEL relative spectral response function for spectral band λ_i. The relative spectral response function has been normalised such that $\int \xi_i(\lambda)\mathrm{d}\lambda \approx \sum_j \xi_i(\lambda_j)\delta\lambda = 1$.

Here the integral $\int E_{\mathrm{FEL}}(\lambda)\xi_i(\lambda)\mathrm{d}\lambda$ has been replaced by the discretised sum $\sum_j E_{\mathrm{FEL}}(\lambda_j)\xi_i(\lambda_j)\delta\lambda$. This is the trapezium rule assumption, considering equispaced data[10], and the difference between the integral and the sum is assumed to be very close to zero. The spectral step size is taken to be 0.1 nm, the step size the relative SRF has been provided in. The (smoothly varying) lamp spectral irradiance has been linearly interpolated to these wavelengths[11].

7.4.2 Results

	Calibration Coefficient	Uncertainty $k = 1$
340		
380	2.22E-09	2.02 %
440	5.73E-10	1.40 %
500	4.46E-10	1.19 %
675	3.19E-10	1.11 %
870	2.55E-10	1.27 %
937	2.44E-10	1.25 %
1020		
1020 (InGaAs)		
1640 (InGaAs)		

7.5 Determining C_{MOON} from C_{SUN} and C_{AUR}

The third method for determining C_{MOON} is by using the calibration coefficients C_{SUN} and C_{AUR} obtained from calibrating directly against the FEL lamp and applying a correction for the MOON gain using the CIMEL specified electrical gain ratios.

Gain pair	Ratio
SUN/MOON & SUN/SKY	4096
SUN/AUR	128
AUR/MOON	32
SKY/MOON	1

Table 9: CIMEL electrical gain ratios

[9] The instrument has a measurement interval (spectral separation of pixels) of 1 nm – 1.5 nm and a bandwidth (spectral response function width for each pixel) of 3 nm to 8 nm depending on wavelength. The data are interpolated to 1 nm steps by the ASD software. However, because the sources being measured with the ASD are similar, the uncertainty associated with these approximations are considered negligible.

[10] For a trapezium rule with equispaced data the first and last step should be multiplied by $\delta\lambda/2$ and intermediate steps by $\delta\lambda$, but given that the spectral response function falls off to zero at both ends, the effect of ignoring this is extremely small (and probably less than other approximations in the trapezium rule).

[11] A comparison was made with different interpolation methods, including a spline fit and dividing the spectral irradiance with the best fit Planck curve (fit to temperature) and then interpolating the result before remultiplying by the Planck curve.

Here, we determine C_{MOON} by using these ratios directly. In Appendix 9A.1 we discuss how we use our own measurements to validate this ratios and calculate an extra uncertainty to apply to the coefficients derived from them.

7.5.1 Results

	$\frac{C_{SUN_{FEL}}}{R_{SUN-MOON}}$	$\frac{C\_AUR_{FEL}}{R_{AUR-MOON}}$
340	5.24E-09	5.33E-09
380	2.21E-09	2.2E-09
440	5.82E-10	5.81E-10
500	4.53E-10	4.51E-10
675	3.25E-10	3.24E-10
870	2.57E-10	2.56E-10
937	2.44E-10	
1020	2.76E-10	2.76E-10
1020	2.14E-10	
1640	4.94E-11	

Table 10: C_MOON determined from C_SUN and C_AUR and their ratios to the MOON gain

7.6 Final MOON calibration coefficients and uncertainties

The final MOON calibration coefficients are combined by weighted mean from all available methods for each filter(see Table 10) Uncertainties are propagated through each method to the final combined standard uncertainty following the GUM guidelines and detailed discussion of this is in project deliverable D4.

Table 11 Final MOON calibration coefficients and associated standard uncertainties

Spectral Channel	MOON calibration Coefficient	Standard uncertainty	Expanded uncertainty $k = 2$
340 nm Si	5.306×10^{-09}	1.72%	3.44%
380 nm Si	2.227×10^{-09}	1.20%	2.41%
440 nm Si	5.759×10^{-10}	0.97%	1.94%
500 nm Si	4.481×10^{-10}	0.96%	1.91%
675 nm Si	3.205×10^{-10}	0.92%	1.85%
870 nm Si	2.547×10^{-10}	0.91%	1.82%
937 nm Si	2.431×10^{-10}	0.97%	1.95%
1020 nm Si	2.735×10^{-10}	1.05%	2.11%
1020 nm InGaAs	2.119×10^{-10}	1.01%	2.03%
1640 nm InGaAs	4.893×10^{-11}	1.06%	2.11%

8 Results Summary and conclusions

The CIMEL photometer calibration for band-integrated irradiance calibration coefficients for MOON gain was determined in four ways:

- A direct calibration against an FEL lamp (FEL399)
- A calibration against a miner's lamp which was itself calibrated against an FEL lamp (FEL401) using an ASD as a transfer instrument
- A calibration against an FEL lamp (FEL399) on the SUN gain, and a correction for the MOON gain using the known gain ratios.
- A calibration against an FEL lamp (FEL399) on the AUR gain, and a correction for the MOON gain using the known gain ratios.

Using the 4 methods we have determined calibration coefficients for the MOON gain along with associated uncertainty. Full discussion of the uncertainty budget can be found in project deliverable D4.

Temperature coefficients have been applied to raw data in laboratory characterisation and will be applied to in situ measurements have been determined at UVa. The coefficients in use at the time of writing (September 2018) are detailed in this report.

We also determined the spectral radiance calibration coefficients for SKY and MOON channels at NPL using a lamp-tile combination. The radiance calibration is not strictly needed for the project but allows cross-check between the calibration and radiometric characterizations of the Cimel photometer carried out at NPL and UVa facilities.

Our results agree within similar percentages to the spread of the results obtained by UVa. Further discussion will be required as to whether this should be looked at in more detail.

9 References

Barreto, A. (2016). The new sun-sky-lunar Cimel CE318-t multiband photometer - a comprehensive performance evaluation. *Atmospheric Measurement Techniques*, 631-654.

CIMEL. (2015, April). CIMEL Multiband photmeter CE318-T.

Manninen. P., H. J. (2006). Determination of distance offsets of diffusers for accurate radiometric measurements. *Metrologia*, 120-124.

Theocharous, E. (2012). Absolute Linearity measurements of PV HgCdTe detector in the infrared. *Metrologia*, S99-S104.

A Appendix

A.1 Validating CIMEL electrical gain ratios.

In section 7.5, the CIMEL specified electrical ratios (SUN/MOON and AUR/MOON are used as a tool for determining MOON calibration coefficients.

Table 12 lists the CIMEL specified electrical gain ratios

Gain pair	Ratio
SUN/MOON & SUN/SKY	4096
SUN/AUR	128
AUR/MOON	32
SKY/MOON	1

Table 12: CIMEL electrical gain ratios

For some sources, source distances and wavelengths, we made measurements under the same conditions for two different gains. From these experimental results we calculated an experimental ratio which could be used to validate the manufacturer specified ratios. Figure 23 to Figure 26**Error! Reference source not found.Error! Reference source not found.Error! Reference source not found.** show the experimentally determined ratios with measurement distance for each gain combination for all measurements.

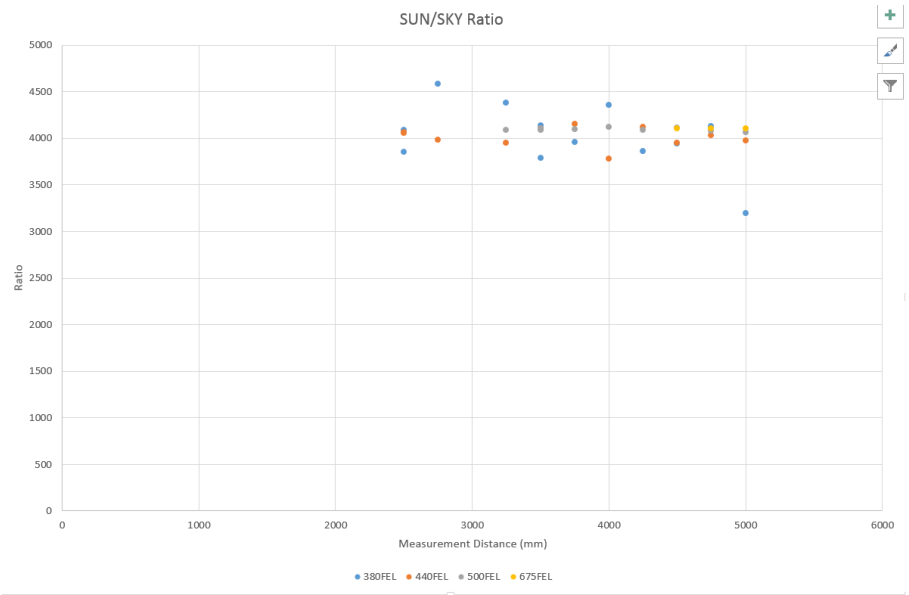

Figure 23: SUN/MOON Electrical Gain ratios

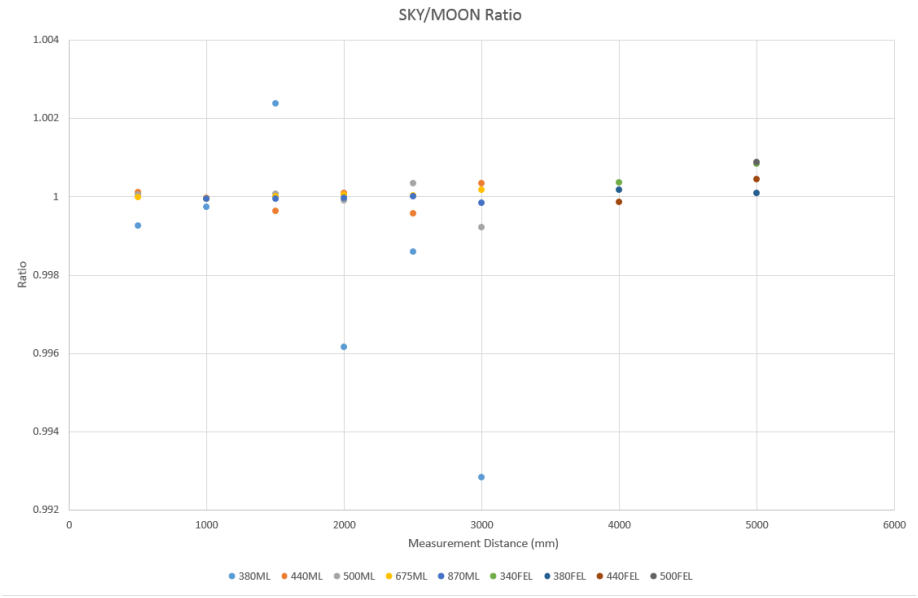

Figure 24: SKY/MOON electrical gain ratios

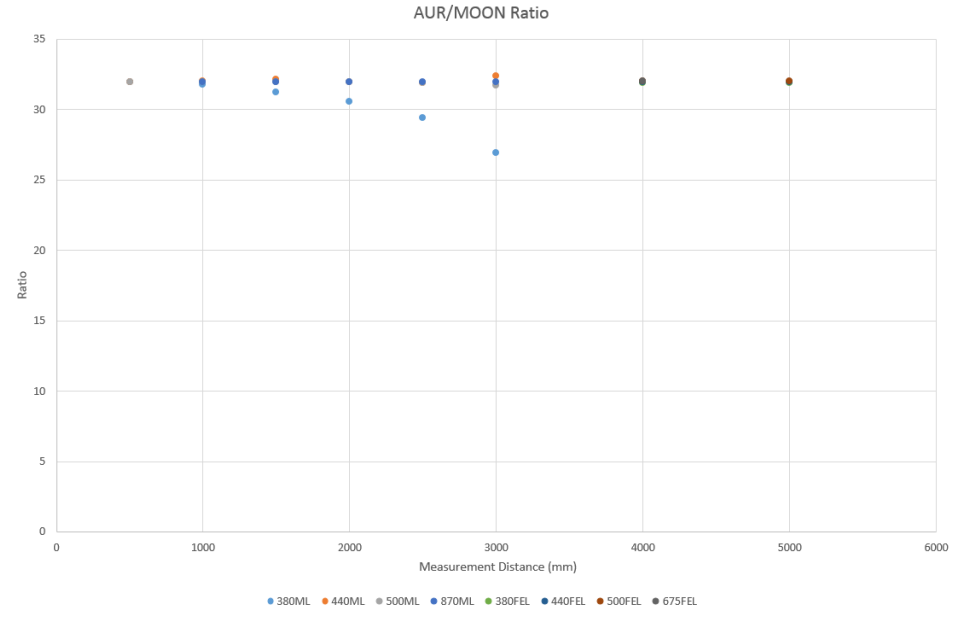

Figure 25: AUR/MOON electrical gain ratios

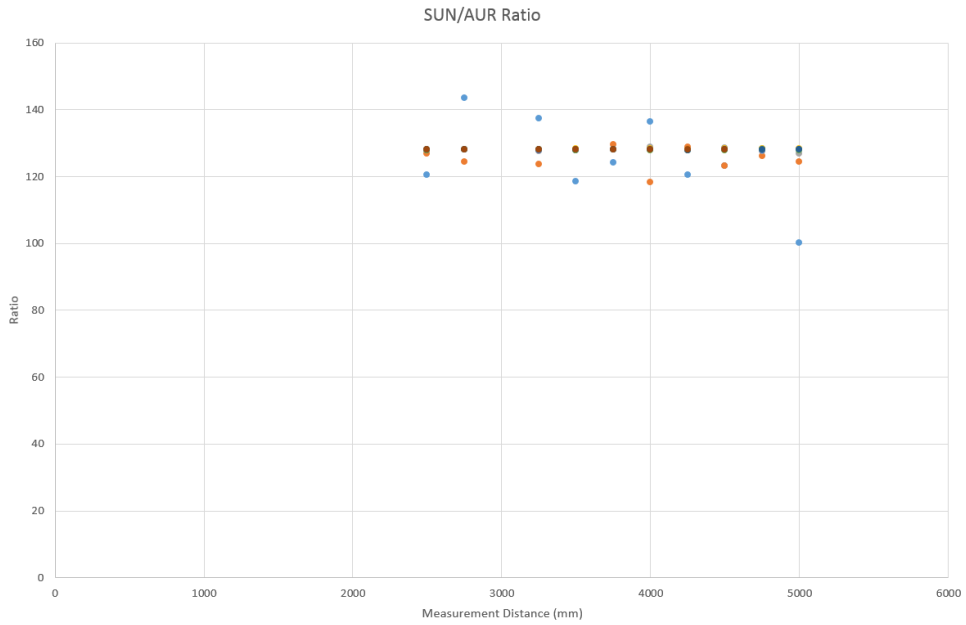

Figure 26: SUN/AUR Electrical gain ratios

For a small number of these measurements, the ratio was different from expected. To test the sensitivity to this we calculated the standard deviation of the triplet of measurements made at each point, and plotted this as a function of signal level (e.g. Figure 27). Based on this we rejected measurements with a standard deviation >0.1 %.

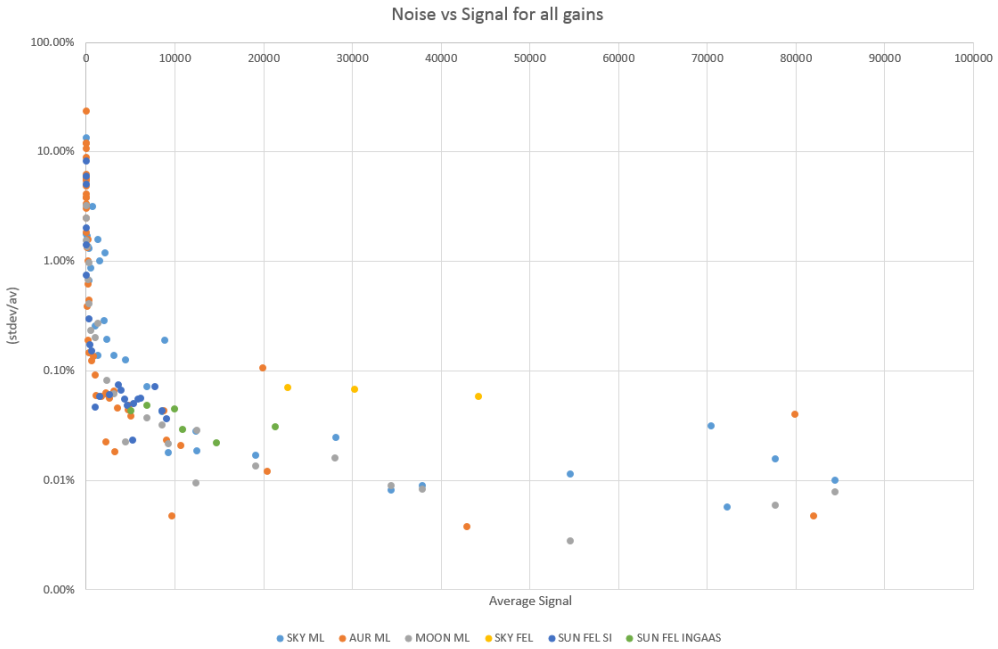

Figure 27: Signal noise as a function of average signal for all gains

Following this we were able to obtain experimental ratios for all gain pairs.

	Experimental ratio	Electrical ratio	Difference
SUN/MOON	4097.75	4096	0.043%
SUN/AUR	128.0388	128	0.030%
AUR/MOON	31.98243	32	0.055%
SKY/MOON	1.000038	1	0.004%

Table 13: Validation of the CIMEL electrical gain ratios

We used the electrical ratio in our analysis, but included the difference between the experimental and electrical ratios as a source of uncertainty (discussion of the uncertainty applied is in project deliverable D4, section 3.5)

A.2 Radiance Responsivity

Determination of the radiance responsivity of the instrument in this section is not used in the lunar irradiance measurements done in this project. They are done only for the sake of comparing radiance calibration approaches (using lamp-tile combination) at NPL and UVa.

The radiance responsivity of the CIMEL photometer was assessed at NPL using a lamp-tile combination. The resulting calibration coefficients for the SKY channel were compared with those calculated by UVa with the use of an integrating sphere and provide opportunity for validation of results obtained at both facilities.

The calibration coefficients for spectral radiance of the CIMEL is given by:

$$C_{\mathrm{CIMEL}}(\lambda_c) = \frac{L_{\mathrm{FEL},\lambda}(\lambda_c)}{D_{\mathrm{CIMEL}_\lambda}(\lambda_c)} \qquad \textit{Equation 17}$$

Where $C_{CIMEL}(\lambda_c)$ is the calibration coefficient for the for the channel c (central wavelength λ_C), $L_{FEL,\lambda}(\lambda_c)$ is the radiance of the FEL lamp used (W m^{-2} nm^{-1}), interpolated to the wavelengths of the CIMEL spectral response function range and $D_{CIMEL,\lambda}(\lambda_c)$ is the digital counts read by the CIMEL.

The spectral response functions used here are those provided by the manufacturer CIMEL, and $L_{FEL_\lambda}(\lambda_c)$ is given by

$$\mathrm{L}_{\mathrm{FEL}\lambda}(\lambda_c) = \frac{\int \xi(\lambda) L_{\mathrm{FEL}}(\lambda) d\lambda}{\int \xi(\lambda) d\lambda} \qquad \textit{Equation 18}$$

Where $\xi(\lambda)$ is the spectral response function for each channel c, and

$$L_{\mathrm{FEL}}(\lambda) = \frac{E_{\mathrm{FEL}}(\lambda)\rho_{\mathrm{tile}(\lambda)}}{\pi} \qquad \textit{Equation 19}$$

$E_{FEL}(\lambda)$ is the source irradiance and $\rho_{tile}(\lambda)$is the reflectance factor of the Spectralon tile, both provided by their respective calibration certificates (calibrated at NPL) with their associated uncertainties and interpolated to the SRF wavelength intervals.

A.2.1 NPL radiance characterisation facility

The “tile” used in the radiance responsivity characterisation is a Spectralon, a diffuse reflectance panel calibrated at NPL at 0°-45°. The lamp is an FEL type (as described in the traceability chain – section 9). The FEL lamp is calibrated at 500 mm, and in this set up the tile will be positioned at 500 mm from the FEL and so no FEL offset need be included in the following calculations.

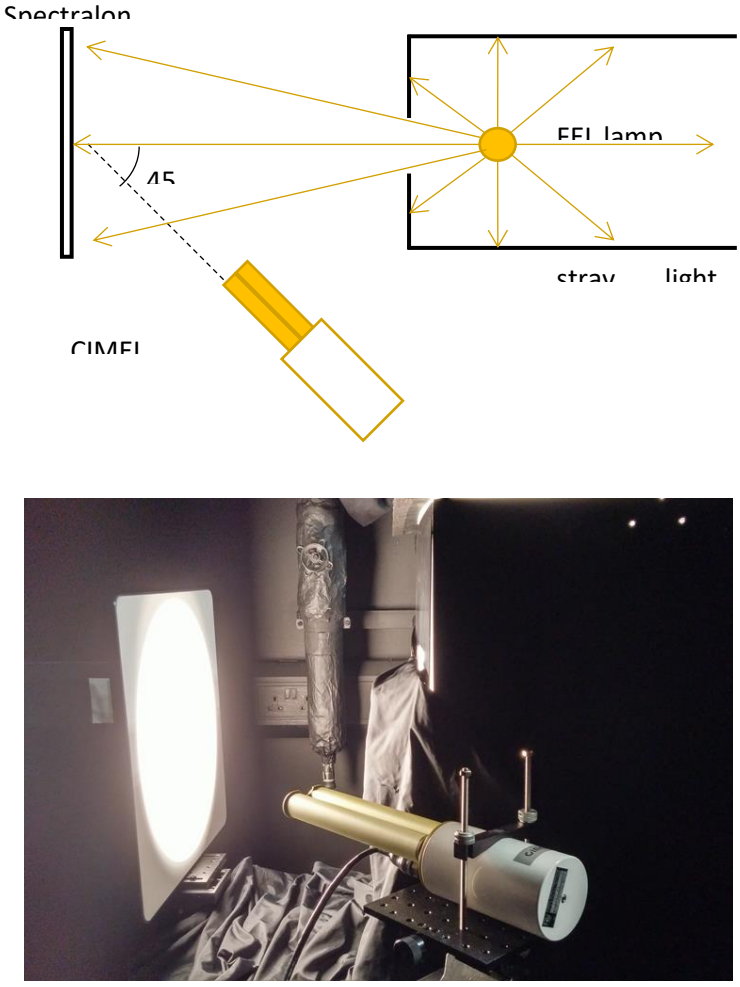

Figure 28: (a) diagram of the lamp-tile experimental setup, (b) photo of a radiance calibration

A.2.2 Radiance results

The signal level achieved from this configuration was appropriate for the MOON and SKY gains. A comparison with SKY calibration coefficients that were determined independently by UVa was also performed as a validation exercise. An associated uncertainty at each wavelength was calculated from contributions from lamp calibration, current setting and alignment as well as the standard error of repeat measurements. The resulting calibration coefficients and their associated relative uncertainties for SKY and MOON channels are presented in Table 16.

When performing an internal validation of the NPL radiance results, the ratio between radiance and sun irradiance calibration coefficients calculated at NPL was observed have what appeared to be an unexpected spectral shape (Figure 29). Separately, the calibration of the tile was under investigation

as it had been the last tile calibrated on the primary reflectance facility before that facility failed. The facility is being upgraded and an improved calibration is expected in early 2019. In the meantime, the tile was recalibrated on a lower-standard "commercial" facility. The resulting calibration coefficients are compared in section A.2.5

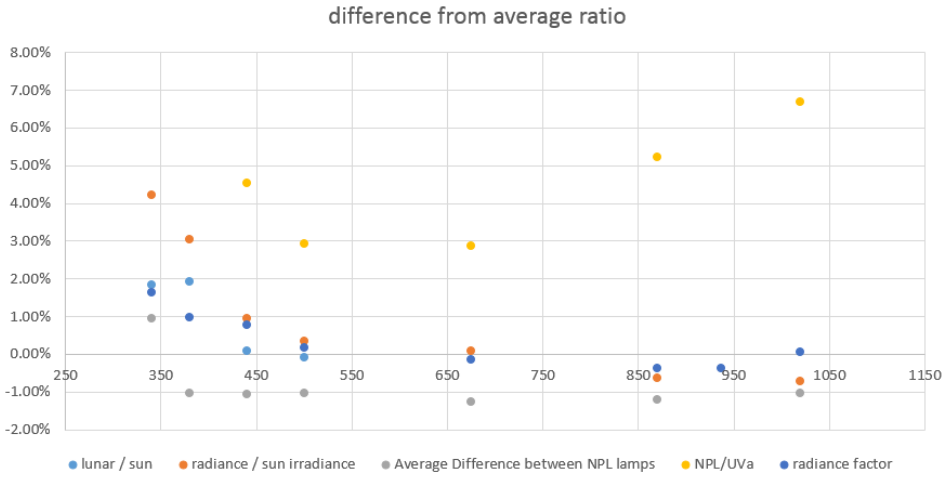

Figure 29: Initial investigation into the NPL radiance calibration results, showing an unexpected spectral shape for the radiance/sun irradiance ratio

A.2.3 Initial Radiance Calibration Results

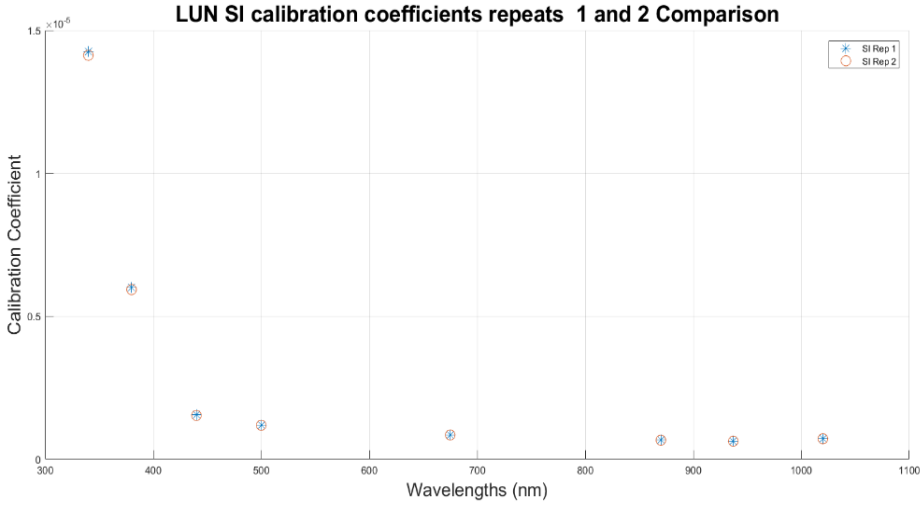

Figure 30: Calibration coefficients for MOON channel SI detector - comparison of repeats 1 and 2

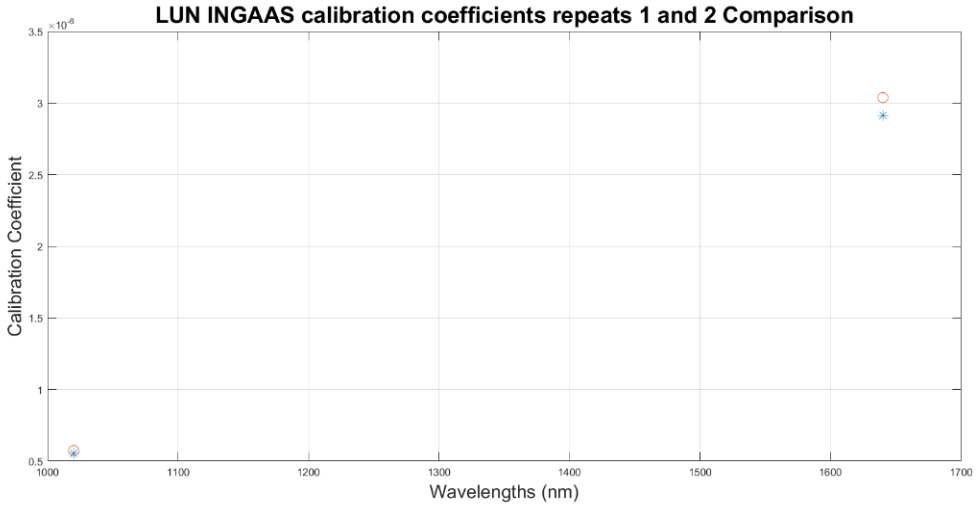

Figure 31: Calibration coefficients for MOON channel InGaAs detector- comparison of repeats 1 and 2

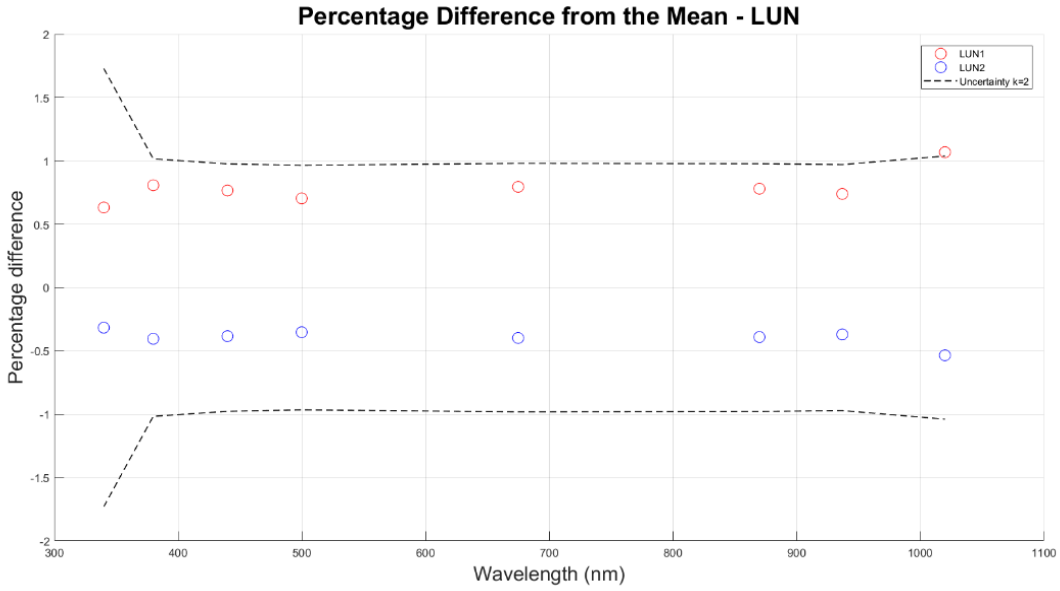

Figure 32: Percentage difference for MOON SI calibration coefficients from repeats 1 and 2, along with associated uncertainty at k = 2

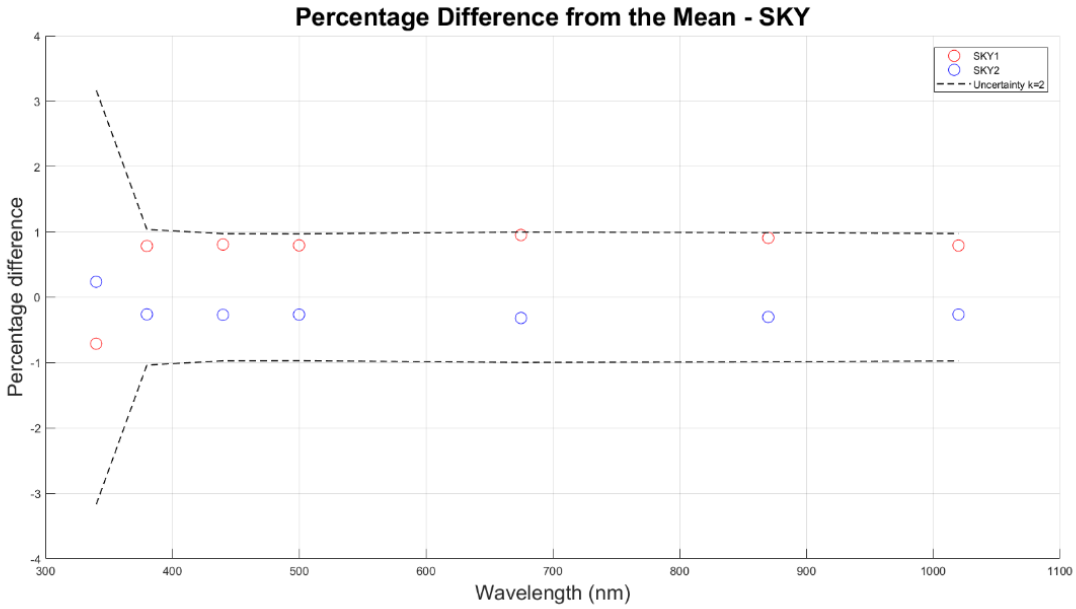

Figure 33: Percentage difference for SKY SI calibration coefficients from repeats 1 and 2, along with associated uncertainty at k = 2

Term	Source of uncertainty	How this can be estimated	Error correlation structures (spectral dimension)
$\boldsymbol{D_{\mathrm{CIMEL,light}}(\lambda_i)}$	Noise (electrical)	Standard deviation of repeat measurements. This is based on multiple sets of repeat measurements to avoid relying on the standard deviation of a small number of measurements.	Fully independent errors – no error correlation in spectral dimension
$\boldsymbol{D_{\mathrm{CIMEL,dark}}(\lambda_i)}$	Noise (electrical)	As above	Fully independent
$\boldsymbol{E_{\mathrm{FEL}}(\lambda)}$	Calibration of the FEL	From calibration certificate. To obtain a standard uncertainty, the calibration certificate uncertainty should be divided by the coverage factor k (usually $k = 2$).	Partially correlated – a full analysis requires understanding the calibration of the FEL, which has been done, but is not repeated here.
$\boldsymbol{E_{\mathrm{FEL}}(\lambda)}$	Representativeness of the calibration of the FEL	The FEL may have changed since calibration due to: • Lamp ageing • Current setting differences • Lamp alignment Uncertainties can be estimated for these effects based on historical experimental evidence and/or laboratory tests.	Fully correlated spectrally. Lamp alignment effects are spectrally neutral. Lamp ageing effects can involve the movement of the filament (spectrally neutral) or a shift in filament resistance. A shift in filament resistance and a lamp current effect will lead to a greater change at short wavelengths than at longer wavelengths (because it is a temperature effect). But – the variability is predictable: that is if you were to know the change at one wavelength you could fully predict the change at other wavelengths. Therefore this error is fully correlated spectrally.

$E_{FEL}(\lambda)$	Distance offset uncertainty	The FEL is calibrated at 500 mm. If used at a different distance, an uncertainty should be added for the distance uncertainty.	This is fully correlated spectrally.
$E_{FEL}(\lambda)$	Spectral interpolation of the FEL spectrum to intermediate wavelengths	A full analysis has not been attempted (yet). Indicative results are obtained through simulation and Monte Carlo Analysis	The spectral error correlation structure is complex. A full analysis will be considered later.
$\xi_i(\lambda_j)$	Uncertainties associated with the estimate of the SRF	We are obtaining the SRF from the manufacturer's measurement. Ideally there will be an uncertainty associated with this, but if not, we can estimate this from our own measurements of similar filters	This is fully independent: the different filters may have independent errors in their estimated SRFs.
ρ_{tile}	Uncertainty associated with tile reflectance factor	From calibration certificate. To obtain a standard uncertainty, the calibration certificate uncertainty should be divided by the coverage factor k (usually $k = 2$).	
$+0$	Assumptions in equation form	Tests of CIMEL linearity Modelling of integration (e.g. through repeating with twice the step size to see what difference it makes)	This is fully correlated between all the silicon channels and independent for the InGaAs channel.

Table 14: Sources of uncertainty for radiance calibration

Table 15: Uncertainty contributions to Radiance calibration

	SKY		MOON		Ratio
	Cal coeff	k=2 unc / %	Cal coeff	k=2 unc / %	SKY/MOON
340	1.451E-05	3.17	1.417E-05	1.73	1.0263
380	5.972E-06	1.04	5.973E-06	1.02	0.9998
440	1.539E-06	0.97	1.536E-06	0.98	0.9987
500	1.194E-06	0.97	1.922E-06	0.97	0.9984
675	8.538E-07	1.00	8.521E-07	0.98	0.9989
870	6.694E-07	0.99	6.683E-07	0.98	0.9987
937	N/a	0.99	6.344E-07	0.97	
1020	7.245E-07	0.97	7.203E-07	1.04	
1020 (InGaAs)			5.63E-07		
1640 (InGaAs)	2.920eE-06		2.98E-06		

Table 16: Calibration coefficients for SKY and MOON channels (original panel reflectance values)

A.2.4 Comparison to UVa calibration coefficients – SKY gain

A comparison between the NPL SKY channel radiance coefficients and those calculated by UVa using the 20" NASA calibrated integrating sphere was performed. The results are presented below. The large difference shown at 380 nm is not unexpected due to the low signal level at this wavelength.

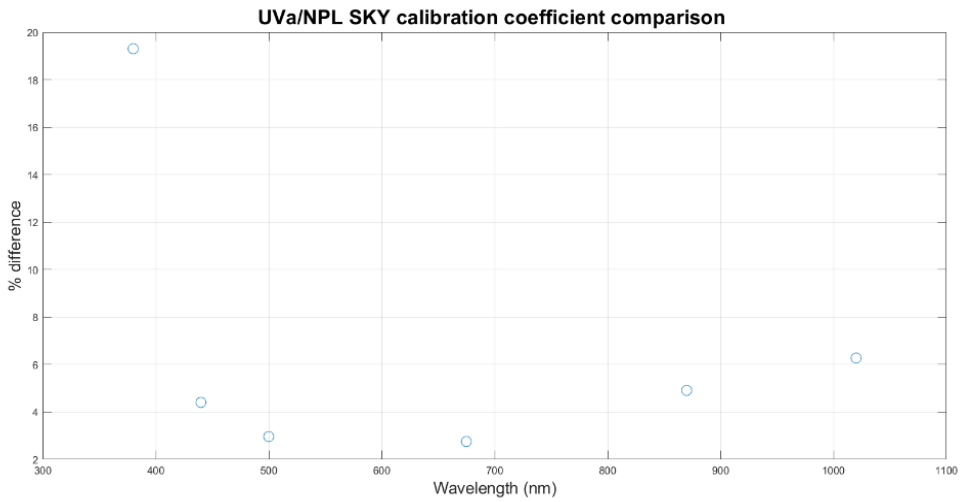

Figure 34: Comparison between NPL and UVa calibration coefficients for SKY channel, SI detector

	SKY		% Diff
	NPL Cal coeff	UVa Cal coeff	
340	1.451E-05		
380	5.972E-06	7.40E-06	19.30
440	1.539E-06	1.61E-06	4.40
500	1.194E-06	1.23E-07	2.96
675	8.538E-07	8.78E-06	2.76
870	6.694E-07	7.04E-07	4.91
937	N/a		
1020	7.245E-07	7.73E-07	6.27
1020 (InGaAs)			
1640 (InGaAs)			

Table 17 : Comparison of NPL and UVa calibration coefficients for SKY channel (original panel calibration)

A.2.5 Results comparison after quick check re-calibration of reflectance panel

A preliminary check on the calibration of the Spectralon panel used in the radiance characterisation has been performed at NPL in September 2018 on the commercial facility covering wavelength range 380-800. This is to check if the Spectralon panel has degraded since its initial calibration.

The resulting calibration coefficients calculated this new data and their relative difference to the UVa coefficients are presented in Table 18.

	SKY		% Diff
	NPL Cal coeff	UVa Cal coeff	
340	1.477E-05		
380	5.979E-06	7.40E-06	19.20
440	1.545E-06	1.61E-06	4.06
500	1.195E-06	1.23E-07	2.83
675	8.525E-07	8.78E-06	2.90
870		7.04E-07	
937			
1020		7.73E-07	
1020 (InGaAs)			
1640 (InGaAs)			

Table 18: Comparison of NPL and UVa calibration coefficients for SKY channel (second panel calibration)

These results show a reduced difference from the UVa coefficients for 3 of the 4 filters with central wavelengths covered by the new panel reflectance calibration. The full re-calibration is due to take place early in 2019.

The difference between the NPL and UVa coefficients is comparable to the relative difference observed between independent calibrations performed at UVa (Table 19)

	SKY			Relative St dev	Relative diff between May 2018 calibrations
	UVa 20" sphere (cal. NASA)	Izaña 8" sphere (cal. NASA)	Izaña 20" sphere (cal. Labsphere)		
340					
380	7.400E-06	6.637E-06	5.700E-06	12.95	15.19
440	1.613E-06	1.616E-06	1.57E-06	1.61	2.86
500	1.232E-06	1.236E-06	1.2E-06	1.6	2.93
675	8.783E-07	8.827E-07	8.5E-07	2.04	3.77
870	7.040E-07	7.048E-07	6.7E-07	2.87	5.06
937					
1020	7.733E-07	7.676E-07	7.2E-07	3.88	6.40
1020 (InGaAs)					
1640 (InGaAs)					

Table 19: UVa SUN radiance calibration coefficients from three independent calibrations

	Previous CC	UVa CC	% Diff	New CC	New % diff	CC % diff
340	1.45E-05			1.45E-05		0.0098%
380	5.97E-06	7.40E-06	19.304%	5.95E-06	19.618%	0.3970%
440	1.54E-06	1.61E-06	4.402%	1.53E-06	4.660%	0.2615%
500	1.19E-06	1.23E-06	2.965%	1.19E-06	3.236%	0.3190%
675	8.54E-07	8.78E-07	2.757%	8.51E-07	3.086%	0.3391%
870	6.69E-07	7.04E-07	4.910%			
937						
1020	7.25E-07	7.73E-07	6.274%			

Table 20: Updated SKY radiance calibration coefficients using September 2018 temperature correction coefficients

	Previous CC	New CC	CC % Diff
340	1.42E-05	1.42E-05	0.0609%
380	5.97E-06	5.96E-06	0.3002%
440	1.54E-06	1.54E-06	0.0600%
500	1.19E-06	1.19E-06	0.0011%
675	8.52E-07	8.52E-07	0.0094%
870	6.68E-07	6.68E-07	0.0066%
937	6.34E-07	6.35E-07	0.0418%
1020	7.20E-07	7.20E-07	0.0108%

Table 21: Updated MOON radiance calibration coefficients using September 2018 temperature correction coefficients